Transcription and potential functions of a novel *XIST* isoform in male peripheral glia

Kevin S. O'Leary [1], Meng-Yen Li [2], Kevyn Jackson [1], Lijie Shi [1], Elena Ezhkova [2], Bernice E. Morrow [1,3], Deyou Zheng [1,4,5,6,*]

1. Department of Genetics, Albert Einstein College of Medicine, Bronx, NY, USA, 10461
2. Department of Stem Cell Biology and Regenerative Medicine, Icahn School of Medicine at Mount Sinai, New York, NY, USA, 10029
3. Departments of Obstetrics and Gynecology, and Pediatrics, Albert Einstein College of Medicine, Bronx, NY, USA, 10461
4. Department of Neurology, Albert Einstein College of Medicine, Bronx, NY, USA, 10461
5. Department of Neuroscience, Albert Einstein College of Medicine, Bronx, NY, USA, 10461
6. Data Science Institute, Albert Einstein College of Medicine, Bronx, NY, USA, 10461

*Corresponding author:

Deyou Zheng, Ph.D.

Department of Genetics

Albert Einstein College of Medicine

Bronx, NY 10461, USA

Deyou.Zheng@einsteinmed.edu

Tel: 718-6781217

Abstract:

The *XIST* RNA is known for its critical roles in X Chromosome inactivation (XCI). It is thought to be expressed exclusively from one copy of the X Chromosome and silence it by recruiting various chromatin factors in female cells. In this study, we find *XIST* expression in male peripheral glia after integrated analyses of single cell RNA-seq data from multiple human tissues and organs. Single cell epigenomic data further indicate that the expression is likely driven by an alternative promoter at the end of the first exon, resulting in at least one shorter transcript (referred to as *sXIST*) that is active in Schwann cells and, moreover, at a higher level in non-myelinating Schwann cells. This promoter exhibits similar activity in female glia. Multiple lines of evidence from bulk transcriptomic and epigenomic data from peripheral nerve tissues further support these findings. Genes co-expressed positively and strongly with *sXIST* in male glia show functional enrichment in axon assembly and cilia signaling, with many of them sharing putative miRNA binding sites with *sXIST*, while the negatively correlated genes are enriched for processes important for neuromuscular junctions. This suggests possible functions of *sXIST* in modulating glia-neuron interactions, perhaps via competitive miRNA binding. This idea is also supported by overexpression analysis of a partial *sXIST* sequence and the finding of significant *XIST* expression changes in human cardiomyopathy and polyneuropathy. In summary, the current study suggests a novel, non-XCI role of *XIST* in peripheral Schwann cells that is mediated by a newly recognized transcript.

Introduction:

X-inactive specific transcript (*XIST*) is a long non-coding RNA that serves as an important regulator of X Chromosome-inactivation (XCI) in mammalian XX females (Loda and Heard 2019). Through interactions between its functional domains (repeat regions A-E) and various proteins, such as Polycomb Repressive Complexes (PRC1/2), CIZ1, and YY1, the *XIST* ribonucleoprotein complex silences one copy of the X Chromosome in female somatic tissues (Loda and Heard 2019; Jacobson et al. 2022). Since the 1990's, *XIST* expression has been continuously shown to be female-specific and exclusively expressed from the inactive X Chromosome in mammals (Borsani et al. 1991; Brockdorff et al. 1991; Brown et al. 1991). It has also been described to unambiguously target the X Chromosome to silence gene expression (Panning 2008; Cerase et al. 2015). However, recent work indicated that *XIST* may also have roles in regulating autosomal genes in female cells (Dror et al. 2024; Yao et al. 2024). Moreover, some studies in cancers further reported that *XIST* could function as a "miRNA sponge" by sequestering multiple miRNAs and thus affecting the expression of their mRNA targets (Marshall et al. 2019; Jiang et al. 2021; Liu et al. 2021; Yan et al. 2022).

Along with these findings of new *XIST* functions beyond XCI, the canonical view of its exclusive expression in female cells has also been challenged. A few studies have reported rare instances of *XIST* expression in male cells, mostly in cancers. For example, two groups independently found *XIST* expression in male samples from multiple types of cancers, such as testicular cancer (Looijenga et al. 1997) and hepatocellular carcinoma (Sadagopan et al. 2022). Similarly, among the 54 human tissues analyzed by bulk RNA sequencing (RNA-seq) in the GTEx consortium from hundreds of healthy individuals (Lonsdale et al. 2013), robust *XIST* expression was observed in the testes and male tibial nerves (Lonsdale et al. 2013; Sadagopan et al. 2022). While *XIST* expression in the testes during spermatogenesis is well-documented (Salido et al. 1992; McCarrey et al. 2002), its regulation and potential function in male tibial nerve remains unexplored. In male cancers, however, Sadagopan *et al*. suggested that *XIST* expression could lead to repression of genes on the X Chromosome (Sadagopan et al. 2022). Thus, additional studies are needed to address whether this occurs in normal human tissues, if repression also occurs for autosomal genes, and if so, in what cell types and to what extent. *XIST*

RNA may have entirely new tissue or cell type-specific roles in males, which further highlights the need for investigation into its non-canonical functions.

Towards this, we performed a systematic analysis of single cell RNA-seq (scRNA-seq) and chromatin accessibility (scATAC-seq) data to characterize *XIST* expression in male and female tissues from healthy human individuals, including data from child and adult heart (Sim et al. 2021; Mehdiabadi et al. 2022; Kanemaru et al. 2023), skeletal muscle (Kedlian et al. 2024), and many other tissues (Zhang et al. 2021). We also analyzed transcriptomic data from multiple studies of mouse peripheral nerves to determine if *XIST*/*Xist* expression in male nerves is conserved. We further performed transcriptomic profiling to characterize genes and pathways that may be affected by the expression of a new *XIST* isoform (termed "*sXIST*") that we discovered in male peripheral glia. Using these systematic approaches, we aim to investigate: a) the cell/tissue type and disease relevance of s*XIST* expression in male cells, b) distinct transcriptional regulation of the *XIST* expression in male and female cells, and c) the potential molecular mechanisms of *sXIST* functions in peripheral glia. The overarching goal is to understand the potential roles of *XIST* in peripheral nerves and its relevance to the functions and diseases of peripheral nervous and cardiovascular systems.

Results:

XIST expression in human male and female Schwann cells

To study the effects of sex chromosomes (XX vs XY) on gene programs in heart tissues at the single cell level, we integrated existing scRNA-seq (or single nucleus RNA-seq, snRNA-seq) data from 20 healthy child and adult human hearts, which were collected from a variety of sources (Sim et al. 2021; Mehdiabadi et al. 2022; Kanemaru et al. 2023) (**Supplemental Table S1**). We unexpectedly observed *XIST* expression in male hearts. To study this in more detail, we clustered the integrated data to define major cell types in human hearts, from which glial (referred to as "neural" in some previous reports) cells were extracted and further subclustered to identify non-myelinating and myelinating Schwann cells (**Fig. 1**) using conventional markers from the literature, such as *SCN7A* and *SLC35F1* for Schwann cells (Karlsson et al. 2021), *NRXN1/2* as pan-glial markers (Diehl et al. 1986), *TUBB3* for neurons (Diehl et al. 1986), and *PLP1* as a myelination marker (Diehl et al. 1986) (**Fig. 1**; **Supplemental Fig. S1**). Based on the

lack of neuronal marker expression, we determined that the previously annotated "neural" cells were glia, in agreement with the authors of the Heart Cell Atlas (Kanemaru et al. 2023). Our analysis showed that male glia expressed *XIST* robustly (**Fig. 1A,B,C**). To study if this is specific to the heart, we then obtained human skeletal muscle scRNA-seq data for fibroblasts and neural cells (Kedlian et al. 2024), with non-myelinating and myelinating Schwann cells annotated by the original authors (**Fig. 1D,E,F**). In both tissues, male glia showed strong *XIST* expression (**Fig. 1C,F**). More specifically, a greater percentage of male non-myelinating Schwann cells (33.63% in heart, 31.13% in skeletal muscle) expressed *XIST* compared to their myelinating counterparts (20.29% in heart, 21.71% in skeletal muscle) (heart: p-value = 1.7×10^{-10}; skeletal muscle: $p < 2.2\times10^{-16}$; Fisher's exact test). The average expression of *XIST* in male non-myelinating Schwann cells was also higher than in myelinating cells, determined at either the single cell level (heart: adjusted p-value = 2.4×10^{-7}, AvgLog$_2$FC (fold-change) = 1.2; skeletal muscle: adjusted p-value = 3.3×10^{-33}, AvgLog$_2$FC = 8.9, Wilcoxon rank-sum test) (**Fig. 1C,F**) or pseudobulk level with cells from the same samples pooled (heart: adjusted p-value = 2.1×10^{-6}, log$_2$FC = 2.8; skeletal muscle: adjusted p-value = $2.8\text{x}19^{-8}$, log$_2$FC = 5.6; negative binomial test). In general, a greater percentage of male glia expressed *XIST* compared to other cell types (< 0.55%) in both datasets (**Supplemental Table S2, Supplemental Fig. S2**). Additionally, even among cell types with *XIST* RNA detected, *XIST* abundance remained significantly lower in the male compared to female glia (**Fig. 1C,F**).

To expand our finding, we analyzed *XIST* expression in the Human Cell Atlas using the CZ CELLxGENE Discover Gene Expression tool (CZI Cell Science Program et al. 2024), which enabled us to quantify the percentages of cells expressing *XIST* across a large number of cell types in aggregated datasets from multiple tissues. Among all the cell types in the atlas, we found significant *XIST* expression in male Schwann cells (58% of 2955 cells) and non-pigmented ciliary epithelial cells (54% of 3011 cells) of the eye, pancreatic stem cells (59% of 492 cells), and fibro/adipogenic progenitor cells of adipose tissue (51% of 1154 cells) (**Supplemental Table S3**). Although *XIST* expression was sporadically detected in other male cell types, these were the only cell types with expression in > 50% of cells, which accounted for just 0.15% (5/3151) of all cell type-tissue combinations that we extracted from the database up to January 2025. There were still only 0.98% (31/3151) of all cell type-tissue combinations if we reduced the detection

percentage to >30%, which was approximately the percentage of male cells expressing *XIST* in the heart and skeletal muscle data (**Fig. 1C,F**). In the central nervous system, 6% of male differentiation-committed oligodendrocyte precursors in both the spinal cord and brain expressed *XIST*, but only 0.4% of mature oligodendrocytes in the spinal cord and 0.3% in the brain expressed *XIST*. Male *XIST* expression was barely detectable in two large cohorts of human brains (Velmeshev et al. 2019; Wamsley et al. 2024).

Taken together, our analysis found that *XIST* is consistently expressed in male Schwann cells, while its male expression in other cell types is much sparser and probably needs stronger evidence from more studies (**Supplemental Fig. S3; Supplemental Table S3**). Note that our finding of *XIST* expression in male cardiac glia was independently described by a recent report from Gorin and Goodman (Gorin and Goodman 2025).

Characterization of XIST transcript sequence and regulation in peripheral nerves

Next, we sought to investigate how *XIST* achieves such specific expression by comparing chromatin accessibility data from Assay for Transposase-Accessible Chromatin using sequencing (ATAC-seq) across cell types. We first turned to scATAC-seq data from the Human Heart Cell Atlas, which were generated using the 10X Multiome platform (Kanemaru et al. 2023). We re-called ATAC-seq peaks using MACS2 (Zhang et al. 2008) for each of the broad cell types defined by the authors, except we renamed their “neural” cells as “glia” because they lacked expression of the neuronal markers in **Figure 1**. This identified two ATAC peaks at the *XIST* locus, with a peak called only for the cardiac glia ~10kb downstream from the main *XIST* promoter. The main *XIST* promoter is constitutively active in female cells but not in male cells (**Fig. 2A**). The glia-specific peak (ChrX:73,841,364-73,841,611; hg38) is located in a region suggested to be an active promoter in several cell lines by the FANTOM5 project. Their data is from a combination of cell lines and tissues (including Schwann cells, optic nerve, and skeletal muscle), with the sample metadata indicating 32% males, 32% females, and 36% as other/NA (Noguchi et al. 2017) (**Supplemental Fig. S4A**). Additionally, the binding sites for a variety of transcription factors (TFs), such as *FOXD3* and *REST*, are found in this region according to motifs in the JASPAR database (Rauluseviciute et al. 2024) (**Supplemental Fig. S4B, Supplemental Table S4**). Among the predicted TFs, one (*FOXO1*) was expressed higher in both

skeletal muscle and heart non-myelinating Schwann cells compared to myelinating, while 11 (*NFATC3*, *SOX13*, *PBX1*, *RREB1*, *SOX10*, *TCF4*, *ETS1*, *SREBF1*, *CEBPB*, *KLF2*, and *ETV5*) were higher in either skeletal muscle or heart non-myelinating Schwann cells. Analysis of the transcription regulatory programs by the SCENIC software predicted that *FOXO1* (and *YY1*) could regulate *XIST* in heart and skeletal muscle Schwann cells, with greater activity in non-myelinating cells (**Supplemental Fig. S5**). This suggests that *FOXO1*, among other TFs, may regulate a previously uncharacterized promoter (or enhancer) of *XIST*.

After separating male from female cells, we observed that all female cell types show high chromatin accessibility at the main *XIST* promoter, consistent with constitutive *XIST* expression in females; however, it became clear that the alternative promoter is likely active in both males and females. Silencing of the main *XIST* promoter in males allowed us to correlate the increased accessibility of the alternative promoter with increased *XIST* expression (**Fig. 2A-B)**. There were significantly more scATAC fragment counts detected over the alternate promoter region (ChrX:73,841,364-73,841,611 +/- 100 bases) in glia compared to all other cell types for both males (p-value = 2.83×10^{-14}, AvgLog$_2$FC = 3.98, Wilcoxon rank-sum) and females (p-value = 1.92×10^{-11}, AvgLog$_2$FC = 2.84, Wilcoxon rank-sum). This was associated with significantly increased *XIST* expression in male glia (p-value < 2.23×10^{-308}, AvgLog$_2$FC = 10.51, Wilcoxon rank-sum test) and to a lesser degree in female glia (p-value = 1.24×10^{-4}, AvgLog$_2$FC = 0.37) compared to all other cell types, likely masked by the higher expression of the full-length *XIST* in female cells.

To study if the newly discovered alternative promoter leads to alternative *XIST* transcripts, we analyzed bulk RNA-seq data because most of the scRNA-seq technologies sequence only the 3' end of RNAs. Unfortunately, we were unable to find bulk RNA-seq data for purified male Schwann cells. Thus, we turned to publicly available bulk RNA-seq data from peripheral nerve samples because this tissue type contains a relatively high proportion of Schwann cells, which are functionally required for supporting/myelinating peripheral neurons. In a previous study, Sandy-Hindmarch *et al*. performed strand-specific bulk RNA-seq on Morton's neuroma and control samples (Sandy-Hindmarch et al. 2025) from males and females independently. These samples were collected from a variety of digital, upper limb, and lower limb nerves, allowing us to examine the distribution of RNA-seq reads along the *XIST* locus in both strands. The data

showed that reads from male samples were significantly enriched at the last exon (i.e., exon 6 at the 3' of *XIST*) (**Fig. S6**). While RNA-seq reads were also mapped to other exons (exons 2-5), only a few reads were aligned to the end of the first exon in males. A comparison of the ratios of RNA-seq reads mapped to the 1st and 6th exons in male and female samples support a significant bias of reads to the latter in males (*p*-value = 0.044, *t*-test) (**Supplemental Fig. S6A**). Importantly, the region at the end of the first exon with only a few RNA-seq reads in male samples is near the cardiac glia-specific accessible region discussed above (**Fig. 2**).

To seek additional, independent support for the activation of the alternative promoter, we next utilized the Cis-element atlas database (CATlas) (Zhang et al. 2021) to study chromatin accessibility for other cell types at the *XIST* locus because it curates comprehensive reference maps of *cis*-regulatory elements from thousands of cell types. Moreover, it has a heart dataset with both snRNA-seq data and scATAC-seq peaks from males and females. We found that cells annotated as "nerve" showed increased chromatin accessibility at the alternative *XIST* promoter, with concordant snRNA-seq reads in the same region, but other cell types did not (**Fig. 3A**).

We also analyzed tibial nerve bulk RNA-seq and ChIP-seq data (two male samples) and sciatic nerve ATAC-seq data (one male sample) available from the ENCODE Project (The ENCODE Project Consortium 2012; Luo et al. 2020). The results support open chromatin accessibility at the alternative promoter, with its activity further supported by active histone modifications H3K4me3 (marks promoters) and H3K27ac (marks both promoters and enhancers). Moreover, the data strongly support that *XIST* expression in males occurred after (3' to) the alternative promoter as seen from enriched signals of RNA-seq and H3K36me3, a histone mark for transcription elongation (**Fig. 3B**). Like in the above analysis of Morton's neuroma data, we again found that RNA-seq reads exhibited a significantly greater bias to exon 6 (vs exon 1) in the male nerve samples when compared to the male brain samples (*p*-value = 0.0011, *t*-test), which do not have Schwann cells (**Supplemental Fig. S7**). This biased trend was also in female data, but the difference was not statistically significant (*p*-value = 0.22).

To address the concern of inferring RNA transcript sequences from short read technology, we searched the ENCODE database for *XIST* transcripts from long-read sequencing technology.

There was no such data from nerve samples, but we found RNA transcripts that aligned with the presence of *sXIST* transcripts in human hearts (**Supplemental Fig. S8**, red arrows; a male and a female sample).

Lastly, for additional regulation evidence, we examined another CATlas dataset derived from integration of multiple male and female tissues and found that adult Schwann cells contained an ATAC-seq peak (called by the authors) at ChrX:73,841,318-73,841,717, which was essentially the exact same region where we called an ATAC-seq peak for cardiac glia (**Fig. 2**). The same peak was called for cardiac fibroblasts, peripheral nerve stromal cells, vascular smooth muscle cells, and type II skeletal myocytes in CATlas (**Fig. 3C**), potentially related to sparse *XIST* expression in non-glial heart cells (**Fig. 1**). Nevertheless, the peaks were the highest in Schwann and peripheral nerve stromal cells. Note that no peak at this region was called for the remaining 106 adult cell types or any of the 111 fetal cell types in CATlas.

Taken together, our systematic analysis uncovers multiple lines of evidence that an alternative *XIST* promoter is active in peripheral glia, most likely Schwann cells, resulting in a shorter *XIST* transcript (or transcripts) in both males and females, which we referred to as *sXIST*.

Functional implications of XIST activation in male Schwann cells/nerves

To study possible roles of s*XIST* expression, we first addressed whether it is involved in repressing X-Chromosome genes in males. We divided the genes on the X Chromosome into groups: genes undergoing X inactivation ("X non-escapees"), genes escaping inactivation ("X escapees") (Wainer Katsir and Linial 2019), and genes in the pseudoautosomal region (PAR) (Weng et al. 2016). As controls, we also included Y Chromosome genes that are not in the pseudoautosomal region (Y non-PAR) and all autosomal genes. We compared their expression between myelinating and non-myelinating Schwann cells using DESeq2 (Love et al. 2014) and the pseudobulking method, dividing samples by sex (**Fig. 4A,B**).

If s*XIST* participates in X Chromosome silencing in males as it does in females, we would expect a general decrease in the expression of X non-escapee genes in male non-myelinating (higher *sXIST*) compared to myelinating Schwann cells, manifesting as a leftward shift in the distributions of their $\log_2$FC values in **Figure 4A,B**. No global shift was observed in the

comparisons of skeletal muscle cells (**Fig. 4A**). Although the mean log_2FC value of this comparison in the heart data was -0.81 with a slight leftward shift (i.e. most non-escapee genes reduced expression in nmSchwann cells), this trend was also seen in our control groups (autosomal genes and X-escapee genes) and similarly in the comparisons of female samples. Thus, it is unlikely that *sXIST* leads to selective repression of X-Chromosome genes. Because male cells have only one X Chromosome, we also expected a decrease in X non-escapee expression in males (leftward shift) when comparing male to female nmSchwann cells. Instead, the distribution of log_2FC values were centered around 0 without apparent skewness for both human and skeletal muscle datasets. The same trends were observed when male and female mSchwann cells were compared. The expected and observed trends are summarized at the bottom of **Figure 4A/B** and the mean log_2FC values for each comparison can be found in **Supplemental Figure S9**. Furthermore, no evidence for a global reduction of non-escapee genes was observed in male or female Schwann cells when compared to all the other cell types (**Supplemental Fig. S10**).

Only PAR genes showed a consistent expression reduction in nmSchwann relative to mSchwann cells in males for both heart and skeletal muscle datasets (shown as left-shift in **Fig. 4A,B** top), indicating a global decrease in PAR gene expression in non-myelinating Schwann cells (heart: mean log_2FC = -0.87; skeletal muscle: mean log_2FC = -0.27). PAR genes are thought to escape XCI (Helena Mangs and Morris 2007), but we found that they exhibited higher expression in males compared to females irrespective of Schwann cell type (**Fig. 4A,B** bottom). This trend appears the same in other tissues from our analysis of bulk GTEx data (Lonsdale et al. 2013) (**Supplemental Fig. S11**). The increased PAR expression in males is consistent with previous reports (Tukiainen et al. 2017). Thus, the increased PAR expression in male compared to female Schwann cells can be attributed to sex biases while decreased PAR gene expression in non-myelinating vs myelinating Schwann cells (in males) may be cell type dependent and related to *sXIST* expression.

In short, we did not find convincing evidence for the involvement of s*XIST* in the general suppression of X Chromosome genes in the male non-myelinating Schwann cells. This contrasts with previous reports in male cancer cells (Looijenga et al. 1997; Sadagopan et al. 2022).

Nevertheless, our results are consistent with the consensus view in the literature that XCI needs the functional domains in *XIST* exon 1 (Brockdorff 2002), which are absent in *sXIST*.

Next, we reasoned that genes potentially affected or regulated by *sXIST* would exhibit a stronger correlation with *XIST* expression in male cells than in female cells because the correlation in female cells captures the combined expression of *sXIST* and the full *XIST* transcript, with the latter at a much higher level, thus masking *sXIST* effects in this analysis. To investigate this, we used the Morton's neuroma bulk RNA-seq dataset from peripheral nerves (Sandy-Hindmarch et al. 2025) discussed above (**Supplemental Fig. S6**) because scRNA-seq data is too sparse for this purpose. We first randomly selected 100 genes and calculated the Pearson correlation coefficients between each of them and all the other human genes across all male (n = 11) and female (n = 22) samples separately to obtain a null distribution defined by fitting an ellipse around 99% of the data points (**Supplemental Fig. S12A-B**). Adding *XIST*, we found that 2.93% of all genes correlated with *XIST* were outside the ellipse (*i.e.*, outliers), compared to just 0.81% in null background (p-value < 2.2×10^{-16}, odds ratio (OR) = 3.68, Fisher's Exact Test), thus representing genes with significantly different correlations with *XIST* between male and female samples. In the end, we determined that 195 genes (0.76% of all genes) had a stronger and positive correlation ("SPC") with *XIST* in males than in females, compared to 0.17% of control gene pairs (p-value < 2.2×10^{-16}, odds ratio = 4.61, Fisher's Exact Test), and 206 genes (0.80% of all genes) had a stronger and negative correlation ("SNC") with *XIST* in males, compared to 0.16% of control comparisons (p-value < 2.2×10^{-16}, odds ratio = 4.92, Fisher's Exact Test) (**Fig. 4C**). Two examples, *DNAAF1* (SPC) and *KCNAB1* (SNC), are shown in **Figure 4D**.

Among the 206 SNC genes, many have roles in neuromuscular system development and function, including *CYFIP2* (involved in synapse formation and plasticity), *FLYWCH1* (linked to neuronal migration and axon guidance), ion channel genes (e.g., *SLC2A4*, *KCNQ4*, *KCNAB1* and *KCNMB1*), calcium signaling genes (*CACNA1S*, CACNA1C and *CACNB2*), extracellular matrix genes (*COL4A2* and *ITGA8*) and genes related to muscle structure and function (*ACTA1/2* and *ACTG2*). Overrepresentation analysis (using ToppFun (Chen et al. 2009)) of the SNC genes also revealed a significant enrichment (adjusted p-value < 0.05) for functions related to muscle system process, calcium ion homeostasis, skeletal muscle development, actin filament-based movement, and action potential (**Fig. 4E**). Among the 195 SPC genes, many have functions in

neurodevelopment and synaptic function (e.g., *FOXP2*, *NPAS1*, and *CNTNAP4*), signaling transduction (e.g., *NFATC1*, *WNT9A*, and *RASGRF2*), ciliary function (e.g., *DNAH9* and *DNAAF1*), and immune response (e.g., *CXCR4* and *IL18*). Unbiased enrichment analysis of the SPC genes showed a significant enrichment of functions related to cilium, extracellular transport, and axoneme assembly (**Fig. 4F**). Although research in this area is relatively sparse, primary cilia are signaling hubs, exist in glia (and neurons), exhibit impairment in some neurodegenerative diseases, and may be involved in a variety of functions related to nerve regeneration signaling in Schwann cells (Ki et al. 2021). Note that neither SPC nor SNC genes were enriched on the X Chromosome and very few exhibited a significant expression difference between male and female samples. Interestingly, both SPC and SNC genes were enriched for putative targets of multiple miRNAs (**Fig. 4E,F**). Previous studies have reported that *XIST* can act as a molecular sponge to inhibit miRNA function (Marshall et al. 2019; Jiang et al. 2021; Liu et al. 2021; Yan et al. 2022), which will lead to a positive correlation among genes sharing miRNA targets because of fewer miRNAs binding to individual targets (Hausser and Zavolan 2014). Among the top 15 miRNAs predicted to target SPC genes, 5 of them (miR-361-3p, miR-32, miR-149-3p, miR-122, and miR-367) have reported evidence for interactions with *XIST* (Li et al. 2018; Cheng et al. 2020; Yang et al. 2020; Jiang et al. 2021; Wang et al. 2023).

To relate this result back to Schwann cells, we wondered how the SPC and SNC genes were differentially expressed between non-myelinating and myelinating Schwann cells. First, we found that two SPC genes (*RNF144A* and *PCBP3*) were significantly upregulated (adjusted *p*-value < 0.05 from DESeq2) when comparing all heart non-myelinating to myelinating Schwann cells. For skeletal muscle, three SPC genes (*CCND3*, *ANO4*, and *PYGL*) were upregulated. For SNC genes, heart non-myelinating Schwann cells showed significant downregulation of 31 (e.g., *ILK*, *FLNA*, and *CYFIP2*) while no SNC genes were downregulated in skeletal muscle. We next used biomaRt to extract all genes in the "epithelial cilium movement involved in extracellular fluid movement" (GO:0003351, 43 genes) and "actin filament-based movement" (GO:0030048, 133 genes) categories because SPC and SNC genes were enriched for these terms, respectively. We used these genes to compute module scores for non-myelinating, myelinating, and "other" glia in the integrated human heart scRNA-seq data discussed above (but not skeletal muscle due to the relatively low number of total Schwann cells). The module scores using the cilia-related

gene set were significantly higher in non-myelinating Schwann cells compared to myelinating and "other" for both males and females (p-value < 0.05, Wilcoxon rank-sum) (**Supplemental Fig. S12C**). However, the module scores using the "actin filament-based movement" gene set were not consistently lower in non-myelinating Schwann cells compared to myelinating (**Supplemental Fig. S12D**).

Overall, these results indicate that *XIST*-expressing male non-myelinating Schwann cells do not exhibit evidence of XCI; instead, they suggest *sXIST* may have other functions potentially involving miRNAs, including some targeting cilia-related genes.

Assessing the effects of sXIST overexpression in a human cell line

To further assess if *sXIST* has non-XCI functions, we over-expressed a subsequence of *sXIST* in a human cell line (HEK-293T), more specifically the second half of *XIST* exon 6 (**Supplemental Methods; Supplemental Fig. S13)**. The construct lacks domain E, which is required for anchoring *XIST* RNA to the inactive X Chromosome through CIZ1 interactions (Sunwoo et al. 2017), and other domains needed for XCI. We carried out strand-specific RNA-seq analysis comparing *sXIST* overexpression ("*XIST* OE") to GFP controls (n=3; **Fig. 5**), and identified a few hundred differentially expressed genes (DEGs), including *XIST* itself (**Fig. 5A,F**; **Supplemental Table S5**). Among the various gene groups described in **Figure 4,** the SPC genes and especially the 10 genes in cilia-related pathways exhibited strong, increased expression in the *XIST* OE samples (**Fig. 5B**). However, the other groups of genes did not exhibit a group-level trend, except for a reduction of PAR genes in males (**Fig. 5B, Supplemental Fig. S13C)**. Thus, our over-expression data are consistent with our bioinformatic results in **Figure 4**.

Functional enrichment analysis of the 318 significantly upregulated (adjusted p-value < 0.05 and fold change > 1.5) and 119 downregulated (adjusted p-value < 0.05 and fold change < -1.5) (**Fig. 5C**) genes showed that the up-regulated set was significantly enriched for GO terms related to cilia and axoneme assembly (**Fig. 5E**). Moreover, "Cilium movement" and "axoneme assembly" were in the top five most enriched GO terms for both male SPC and *XIST* OE upregulated genes. Four upregulated genes (*BDKRB2*, *DNAAF1*, *DNAI3*, and *LRRC46*) and two downregulated genes (*COL4A6*, and *P2RX1*) in our over-expression analysis overlapped with SPC and SNC

genes, respectively. The small overlap potentially reflects distinct biological contexts of HEK-293T cells and peripheral nerves.

Targets of multiple miRNAs were enriched in the upregulated genes. Importantly, among the top 20 miRNAs, miR-9, miR-651, miR-520a-5p, and miR-218-2 (also called miR-218-3p) were predicted by miRDB (Chen and Wang 2020) to bind to the overexpressed s*XIST* sequence, as was miR-520a-3p but not ranked in the top 20. MiR-9-5p is especially interesting because it is expressed in both HEK-293T (Kavakiotis et al. 2022) and nerve tissue (Rishik et al. 2025), previously implicated in *XIST* sponging (Zheng et al. 2020), and inhibits Schwann cell migration (Zhou et al. 2014). One of its predicted targets is *HMMR* (hyaluronan-mediated motility receptor; **Fig. 5F,G**), which is highly expressed in Schwann cells (Ouasti et al. 2020), important for their motility (Ouasti et al. 2020), plays a role in mitotic spindle positioning (Connell et al. 2017), and supports neural development (Connell et al. 2017). While not predicted to bind to its 3' UTR, a potential hsa-miR-9-5p binding site is found in the final exon of *DNAAF1* (**Fig. 5G**), a cilia-related gene strongly correlated with *XIST* expression in males (**Fig. 4E**). It has been implicated in neural tube defects (Miao et al. 2016) and ciliary dyskinesia due to its important role in dynein-arm complex assembly (Loges et al. 2009).

As for the other miRNAs, cilia-related genes are predicted targets of miR-520a-5p (*DNAH6*, *DNAI4*), miR-651 (*DNAAF1*), miR-218-2 (*DNAAF1*), and miR-520a-3p (*DNAAF1*). Mir-218-2 and miR-34a-5p were also predicted to target *LRRC46*. Additionally, miR-520a-5p, miR-9, and miR-34a have been previously implicated in *XIST* sponging (Liu et al. 2018; Zheng et al. 2020; Liu et al. 2021). To check if these miRNAs are expressed in HEK-293T cells and nerve tissue, we searched the microRNA Tissue Expression Database (Kavakiotis et al. 2022) and confirmed that miR-218-2-3p, miR-34a-3p/5p, miR-651-3p/5p, and miR-9-3p/5p were expressed, with miR-9 showing the strongest expression (top 3% of 1773 expressed miRNAs in 293T cells and top 1% of 1089 expressed miRNAs in peripheral nerves). These miRNAs were also detected in nerve tissue according to the miRNA Tissue Atlas (Rishik et al. 2025).

Taken together, many genes, including those related to cilia, were upregulated upon overexpression of an s*XIST* fragment and there is no evidence that the DEGs are enriched on the

X Chromosome. The overexpression data, however, supports the potential function of *sXIST* as a miRNA sponge.

Evaluating XIST expression in glial cells from human cardiomyopathy and polyneuropathy tissue

Since *sXIST* exhibited high expression in male Schwann cells, and because Schwann cells are part of the intracardiac nervous system and important for cardiac sympathetic nerve fasciculation (i.e., axon bundling to form nerve tracts) (Hortells et al. 2021), we wondered whether there might be changes in *XIST* expression in the glia of diseased hearts, more specifically from patients with arrhythmogenic cardiomyopathy and dilated cardiomyopathy (up to 38% of hearts with dilated cardiomyopathy exhibit non-sustained ventricular arrhythmias (Spezzacatene et al. 2015)). We thus analyzed a snRNA-seq dataset with 881,081 nuclei from 18 healthy and 61 non-ischemic, failing hearts (Reichart et al. 2022) (**Fig. 6A**). We again found that author-annotated male "neural" cells, which we reclassified to glia based on marker gene expression (**Supplemental Fig. S14**), expressed *XIST* at much higher levels compared to other male cell types (adjusted *p*-value $< 2.23\times10^{-308}$, $\log_2$FC = 6.44, Wilcoxon rank-sum) (**Fig. 6B**). We also found that the percentage of cells expressing *XIST* in glia was significantly higher in both cardiomyopathy groups for males and females (*p*-value $= 2.2\times10^{-16}$, OR = 1.14, Fisher's exact test**)** (**Fig. 6D**). After pseudobulking by samples, the expression difference of *XIST* between disease groups and controls was only significant for males (**Fig. 6C**). High expression of the full-length *XIST* transcript in female samples could explain the inconsistency in the results from pseudobulk level and single cell level, since *sXIST* would contribute to a fraction of the total pseudobulked expression values.

Because of *XIST* upregulation in cardiomyopathy, we expected that SPC genes would be upregulated and SNC genes downregulated (**Fig. 4**) in both types of cardiomyopathies. We found this to be true for five genes, which were *RYR2*, *TPM2*, *CACNB2*, *AKAP6*, and *MYOCD*. A full list of the overlap between disease DEGs by SPC/SNC genes, sex, and expression direction relative to normal hearts is provided in **Supplemental Table S6**. We also observed significant differences in *FOXO1* expression, mentioned above as a potential TF regulating *sXIST* expression (*FOXO1* expression was significantly higher in male and female disease group glia, except female arrhythmogenic RV cardiomyopathy) (**Fig. 6E**). *COL4A6*, which is an SNC gene

(**Fig. 4**) and downregulated in the *XIST* OE group (**Fig. 5**), showed decreased expression in male and female dilated cardiomyopathy glia compared to healthy hearts (**Fig. 6F**). *RYR2*, another SNC gene that encodes a receptor crucial for cardiac muscle function and involved in cardiac and neuronal disorders (ryanopathies) (Sleiman et al. 2021), was significantly downregulated in both types of cardiomyopathies for male and female glia (**Fig. 6G**).

For males and females, we also used SPC and SNC genes to compute module scores for glia from cardiomyopathy and healthy groups. For males, the SPC module scores, as expected, were significantly higher (Wilcoxon rank-sum test p-value < 0.05) in glial cells from both types of cardiomyopathies compared to controls (**Fig. 6H**). For females, module scores were higher for glial cells from arrhythmogenic RV cardiomyopathy but not dilated cardiomyopathy (**Fig. 6H**). For both males and females, SNC gene module scores were significantly lower in glial cells from both cardiomyopathies compared to healthy controls (**Fig. 6I**).

Likewise, we studied *XIST* and its putatively affected pathways using scRNA-seq data comparing polyneuropathy (PNP) sural nerve samples to controls, which included non-myelinating, myelinating, and repair Schwann cells (Heming et al. 2025). We found that *XIST* was significantly downregulated in non-myelinating Schwann cells from PNP samples (adjusted p-value = 2.98×10^{-2}, AvgLogFC = -1.91, two-sided likelihood ratio test) but not in myelinating or repair Schwann cells (**Supplemental Fig. S15, Supplemental Table S7**). Heming *et al*. noted that genes upregulated in non-myelinating Schwann cells from PNP samples were associated with cell migration (Heming et al. 2025). We further found that the average log fold change value for genes in the actin filament-based movement (GO:0030048) gene set was 0.56 (high in PNP) comparing PNP non-myelinating Schwann cells vs controls, while the average log fold change values for cilium-related genes (GO:0003351) was -0.19 (lower in PNP).

Overall, our results indicate that peripheral glia from diseased tissue exhibit significant changes in *XIST* expression, but the direction of change depends on the disease (lower in PNP and higher in cardiomyopathy), suggesting that *XIST* (specifically *sXIST* since it is the only apparent transcript in male hearts) could potentially affect the expression of some genes implicated in heart disease and neuropathy.

Xist expression in mouse male glial cells

To determine if *Xist* expression is conserved in male mouse Schwann cells, we focused on mouse scRNA-seq data from peripheral nerves (Gerber et al. 2021; Yim et al. 2022). The data were collected after male (n=2) and female (n=2) samples were pooled; thus, sex information was not available for individual cells. We therefore used Y Chromosome gene expression to predict sex, similar to the method described by Twa et al. (Twa et al. 2024). We found that labeling cells with any non-pseudoautosomal Y Chromosome gene expression as from males was 91.18% accurate using human skeletal muscle cells and 75.95% accurate using human heart cells (**Supplemental Fig. S16**), but our method is expected to put many true male cells into the female group. We applied this strategy to separate male cells in the scRNA-seq data collected by Gerber *et al*. for peripheral nerves at postnatal day 1 (P1) and 60 (P60). The authors had identified Schwann cells, so we retrieved these cells from their full data and then subclustered. A cell type in P1 called fibroblast-related (FbRel) also expressed Schwann cell-related genes and were therefore included. For both P1 and P60 data, we used the same myelin-related genes in **Figure 1** (*PLP1*, *MPZ*, *MBP*, and *PRX*) to separate cells into myelinating vs non-myelinating cells. It is important to note that all clusters expressed myelinating genes to some degree, but those with lower expression were called non-myelinating Schwann cells (**Supplemental Fig. S17A-B**). The second dataset from Yim *et al*. already had myelinating and non-myelinating Schwann cell subtypes separated, so we directly compared cells in these two subtypes after predicting male and female cells (**Supplemental Fig. S17C**). We should also note that the P60 sciatic nerve sample had only 414 Schwann cells compared to 3,443 at P1 and 9,676 for other peripheral nerves.

The predicted male Schwann cells from both studies expressed *Xist*, indicating co-expression of *Xist* and Y Chromosome gene(s) in the same cells. Non-myelinating Schwann cells had the greatest percentage of male cells expressing *Xist* in all three groups of samples (**Supplemental Fig. S18, S19**). Yim *et al*. data exhibited greater between-sample variation in the percentage of cells expressing *Xist* by cell type for both males and females (**Supplemental Table S8, Supplemental Fig. S19**). A summary of these comparisons for each sample is in **Supplemental Table S9**, which supports higher *Xist* expression in the non-myelinating compared to myelinating Schwann cells (**Supplemental Fig. S18A-C**), consistent with the human data (**Fig. 1**). Gerber *et al*. also provided a tool for their scRNA-seq sciatic nerve atlas (SNAT) data for visualizing gene

expression through mouse age and pseudotime by cell type in their Smart-seq2 data. Although *Xist* was not detected in the Smart-seq2 samples (perhaps a technical effect), *Foxo1* (predicted by SCENIC to regulate *XIST* in humans) exhibited higher expression in non-myelinating glia, showed greater expression with increasing mouse age, and demonstrated increasing expression through pseudotime for non-myelinating glia but not myelinating glia (**Supplemental Fig. S20**). *Foxo1* expression was also higher in predicted male and female non-myelinating Schwann cells in the mouse data we analyzed (**Supplemental Fig. S18**).

To expand our analysis to other mouse tissues, we again utilized the CZ CELLxGENE Discover Gene Expression tool (CZI Cell Science Program et al. 2024) to determine the percentage of male and female cells expressing *Xist* in mice by cell type across tissues (**Supplemental Fig. S3B**). Across all tissues, cells in the eye had a particularly high percentage of male cells expressing *Xist*, especially for amacrine cells (45%) and retinal ganglion cells (34%). Several other amacrine cell subtypes also had a high percentage of male cells expressing *Xist* as well as "neural" cells of the eye (7%), which may be glia. A summary of CELLxGene percentages by cell type for mice can be found in **Supplemental Table S10**.

Taken together, our analysis of mouse RNA-seq data indicate that, like humans, male Schwann cells express *Xist* with a bias toward the non-myelinating lineage. The *Xist* expression in mouse male peripheral glial cells, however, seems less specific than in human data. At this point, it is unclear if this represents a true species difference or a bias in sampling.

Discussion

XIST is the most studied long non-coding RNA (lncRNA) whose main and canonical functions, interacting proteins, and individual functional domains have been dissected by many previously published works. In this study, we found that a shorter *XIST* isoform is expressed in male Schwann cells in both healthy and disease conditions, with its level higher in non-myelinating Schwann cells. Our findings challenge the idea that *XIST* is exclusively female-specific in non-cancerous cells, while our results support potential non-XCI roles of *XIST* in both male and female peripheral glia cells.

Our data indicate that *XIST* expression in male Schwann cells is driven by a previously uncharacterized promoter at the end of the first exon, leading to a shorter *XIST* RNA. This is based on multiple lines of evidence, including RNA-seq read coverage, H3K36me3 modification, and long-read full-length transcripts. We believe this short *XIST* isoform is also expressed in females based on shared scATAC-seq peaks across datasets and long-read RNA-seq data from the heart; however, high expression of the full-length isoform makes it impossible to conclude unambiguously if the same short transcript is present in both male and female glia. Furthermore, although our presentation considered one short isoform, *sXIST*, our data do not exclude the possibility that multiple short, spliced isoforms exist in the Schwann cells since our current data did not have the resolution to resolve alternative splicing. Distinct *XIST* isoforms have been reported (Johnston et al. 1998; Memili et al. 2001; Yue and Ogawa 2018), but the documented isoforms are not related to *sXIST* reported here. We should also mention there is some degree of *sXIST* expression variations across human individuals from whom all the bulk or single cell data were derived. In addition to technical reasons, one possibility is that the tissue samples could have different composition of non-myelinating Schwann cells or moreover *sXIST* expression is affected by the activation state of Schwann cells.

Our finding brings up more questions than we could address here. The central question is whether *sXIST* has a non-XCI functional role in Schwann cells, and more generally in peripheral nerves, or if its expression is merely transcriptional noise. Since the *sXIST* transcript(s) does not contain the tandem repeat domains required for XCI, we think its expression does not lead to XCI, supported by our analysis and data. Instead, we suggest that *sXIST* RNA may regulate the expression of autosomal genes involved in cilia-related processes and others that are important for neuromuscular development and in male and female peripheral nerves. LncRNA functions, however, are diverse and challenging to define (Statello et al. 2021; Mattick et al. 2023). Among many other potential mechanisms, we suggest that *sXIST* could act as a miRNA sponge. This hypothesis also considers the possibility of *sXIST* RNA existing as circular RNAs (circRNAs) because it contains short repeat sequences. In fact, many circRNAs mapped to the locus are recorded in the circAtlas (Wu et al. 2020), e.g., *hsa-XIST_0011*. Therefore, it is possible that *sXIST* RNAs can sequester miRNAs that target genes in processes important for non-myelinating Schwann cell functions, such as cell-cell signaling through primary cilia, which exist in glia and

may be involved in a variety of functions related to nerve regeneration signaling (Ki et al. 2021). This is in line with the main functions of Schwann cells in supporting nerve development and regeneration after injury. We also noticed that many zinc-finger transcription factors were up-regulated in our *sXIST* overexpressing cells (**Supplemental Fig. S13E**), but the functional implication is unclear.

Among the top 15 miRNAs predicted to target SPC genes, 5 of them (miR-361-3p, miR-32, miR-149-3p, miR-122, and miR-367) have been reported to interact with *XIST*, although in those studies the specific *XIST* isoforms were not addressed and were all in cancer contexts (Li et al. 2018; Cheng et al. 2020; Yang et al. 2020; Jiang et al. 2021; Wang et al. 2023).

From our s*XIST* overexpression data, we similarly found that three miRNAs (miR-520a-5p, miR-9, and miR-34a) predicted to target upregulated genes were previously reported to interact with *XIST*, with miR-520a-5p described in non-small cell lung cancer resistance (Liu et al. 2021) and miR-34a in thyroid cancer (Liu et al. 2018). As for miR-9, it is a known regulator of neurogenesis (Coolen et al. 2013), was shown to inhibit Schwann cell migration (Zhou et al. 2014), and is targeted by *XIST* to regulate mesenchymal stem cell differentiation in the bone marrow (Zheng et al. 2020). If *XIST* acts as a sponge for miR-9, its downregulation in neuropathy (**Figure S15**) may exacerbate symptoms because the excessive miR-9 could lead to reduced Schwann cell migration to damaged nerves. It is therefore compelling that *HMMR* (also known as *RHAMM* or *CD168*) shares a binding site with miR-9-5p at its 3' UTR (**Fig. 5G**). *HMMR* is important for the motility of Schwann/Schwann-like cells (Ouasti et al. 2020) and is involved in the PLK1-dependent pathway that stabilizes astral microtubules coming from the centrosome (Connell et al. 2017). Centrosomes and the microtubules they produce are important for primary cilia development (Dantas 2020), so we wonder if *HMMR* and other cilia-related genes affected by *XIST* expression could affect primary cilia production/maintenance.

Future studies are needed to address this and, more importantly, whether these miRNAs and others predicted from our analysis bind to s*XIST* RNA in Schwann cells and lead to altered expressions of their other targets, either at the transcript or protein level. We should note that miRNAs can regulate their targets both negatively and positively (Hausser and Zavolan 2014).

It is important to point out that the model of *XIST* functioning as a miRNA sponge will depend on its location in the cytoplasm, but some miRNAs are located in nuclei (Marshall et al. 2019; Morey et al. 2025). The full length *XIST* RNA contains sequences that retain it to nuclei, but these sequences are mostly absent in the *sXIST* transcript. Thus, although we did not have data to resolve the sub-cellular location of *sXIST* RNA, conceivably it can be in the cytoplasm, nucleus, or both (Politz et al. 2006; Leung 2015; Turunen et al. 2019). Future studies will be needed to pinpoint *sXIST*'s cytoplasmic and/or nuclear distribution and determine its direct interactions with key miRNA targets.

Our finding of *XIST* expression changes in cardiomyopathy and polyneuropathy is also interesting. *XIST* and its miRNA sponging capacity are suggested in a variety of cardiovascular/circulatory system-related diseases, such as myocardial ischemia, cardiac hypertrophy, myocardial infarction, atherosclerosis, deep vein thrombosis, pulmonary arterial hypertension, and more (Almalki 2024). Gorin and Goodman similarly showed that *XIST* expression was higher in cardiomyopathy (Gorin and Goodman 2025), but we are unaware of other literature directly linking *XIST* to this disease. Our results revealed that *RYR2*, which exhibited greater negative correlation with *XIST* in male peripheral nerves and therefore may be (either directly or indirectly) downregulated by the *sXIST* transcript, was significantly downregulated in glial cells of cardiomyopathy hearts. Because *RYR2* is an important cardiac muscle-related gene involved in multiple diseases (Sleiman et al. 2021), we wonder whether ryanopathies are partly influenced by aberrant *sXIST* expression. If so, specifically targeting *sXIST* could upregulate *RYR2* and modulate disease progression. However, more work is needed to prove that *sXIST* directly influences *RYR2* expression.

Another critical question is whether the expression, regulation and function of *XIST* is conserved across mammalian species. We tried to address this, but mining sex-specific gene expression from published mouse RNA-seq data is extremely difficult because almost all studies pool tissues from both sexes. We attempted to overcome this limitation by predicting the sex of individual cells, but the approach will not work for bulk RNA-seq data. Based on our analysis and some limited data in the mouse ENCODE Project, we are confident that *Xist* is expressed in

peripheral nerves in male mice, but we cannot determine if the alternative promoter and resulting transcript(s) are conserved between humans and mice.

Finally, our analysis of the CELLxGENE data indicated that several other cell types, such as pancreatic stem cells, ciliary epithelial cells, and fibro/adipogenic progenitor cells also exhibit active *XIST* expression in male cells. In future studies, we need to address if *sXIST* is activated and functional in these cell types like in Schwann cells.

In conclusion, our study suggests that *sXIST* is highly specific to peripheral glia and potentially acts as a molecular sponge to sequester miRNAs that are involved in modulating various Schwann cell functions. Further work is needed to confirm the exact region of *sXIST* that regulates the expression of nervous system-related processes and whether this indeed occurs through miRNA binding. While we focus our discussion on miRNA sponge function in this study, the *XIST* functions in peripheral glia are very likely more complex. For example, we do not know if the short and full *XIST* transcripts interact in female cells.

Methods

Overexpression of sXIST in the HEK-293T cell line and RNA sequencing

The last 3,323 base pair (bp) sequence of *XIST* exon 6 (ChrX:73,820,656-73,823,979(-)) was cloned into pLV-eGFP vector and transfected into *HEK*-293T cells for overexpression. Total RNA was isolated from the *sXIST* overexpression cells and controls for strand-specific RNA sequencing (see **Supplemental Methods**). RNA-seq reads were mapped to the human genome (GRCh38) with the GENCODE annotation (v46) (Mudge et al. 2025) by the STAR aligner (v2.7.9a) (Dobin et al. 2013). Gene counts were determined using RSEM (v1.2.28) (Li and Dewey 2011). Differential expression analysis was performed using DESeq2 (Love et al. 2014).

Public bulk and single cell data

Human peripheral nerve bulk RNA-seq data: The data were collected by Sandy-Hindmarch *et al*. from 11 controls (4 females, 7 males) and 21 Morton's neuroma samples (18 females, 4 males) to understand the molecular signatures of nerve injury (Sandy-Hindmarch et al. 2025). All Morton's neuroma samples were from the plantar digital nerves whereas control samples were

collected from a variety of upper and lower limb nerves (3 plantar digital, 3 gracilis motor, 4 posterior interosseous sensory, and 1 intercostal sensory). We downloaded the raw count expression data and FASTQ files (generated from strand-specific RNA sequencing) from the Gene Expression Omnibus (GEO): accession number GSE250152. We mapped the RNA-seq reads with STAR (Dobin et al. 2013) to the GRCh38/hg38 genome build, as the authors did. The alignment BAM files for individual samples were then merged by sex and neuroma status and subsequently indexed using SAMtools v1.14 (Danecek et al. 2021). Then reads mapped to the *XIST* locus (Chr X:73,820,656-73,852,714) were extracted and visualized in IGV (Robinson et al. 2011). For expression difference between the 1st and 6th exon, the number of reads were obtained using SAMtools for exon 6 (ChrX:73,820,548-73,828,166) and exon 1 (ChrX:73,841,317-73,852,768) for each sample. The ratios of the exon 6 reads to exon 1 reads for male and female samples were compared by *t*-tests.

Human tibial and sciatic nerve bulk RNA-seq, ATAC-seq and ChIP-seq data: The data were downloaded from the ENCODE Project (The ENCODE Project Consortium 2012) data portal, including RNA-seq and ChIP-seq (H3K4me3, H3K4me1, H3K27ac, H3K36me3, H3K27me3, and H3K9me3) data from the tibial nerve of 37 and 54-year-old males, and ATAC-seq data from the sciatic nerve of a 26 year-old male and 16 and 47-year-old females. For positive (+) and negative (-) strand RNA-seq bigWig files, we used bigWigSummary from the UCSC Genome Browser (Perez et al. 2025) to get the average signal for exon 6 (ChrX:73,820,548-73,828,166) and exon 1 (ChrX:73,841,317-73,852,768), which we then multiplied by the exon length to get the total signal. We used these signal values to calculate the ratio of exon 6 to exon 1 signal for each strand and sample. The accession numbers for the data used for results presented in **Figure 3** and **Supplemental Figure S7** are listed in **Supplemental Table S1**.

Human heart long-read RNA-seq data: The data were downloaded from the ENCODE Project (The ENCODE Project Consortium 2012) data portal. BAM files for accession numbers ENCFF330VRX and ENCFF327SFR were downloaded and filtered for reads on the X Chromosome.

Human heart sc/snRNA-seq data: The data were from three difference sources (Sim et al. 2021; Mehdiabadi et al. 2022; Kanemaru et al. 2023) (**Supplemental Table S1; Supplemental**

Methods). These three datasets were re-analyzed using Seurat (Hao et al. 2024) (version 5) to manage sample-level metadata (age/age range, sex, and dataset) and filter for cells/nuclei with > 200 detected genes and percent mitochondrial gene expression < 10% for scRNA-seq data and 5% for snRNA-seq data. Next, we normalized raw counts for all sc/snRNA-seq data with Seurat's NormalizeData function, followed by FindVariableFeatures, ScaleData, and RunPCA functions. We also used Scrublet (Wolock et al. 2019) to predict and remove doublets from these data. Next, we used reciprocal principal component analysis (RPCA) (Hao et al. 2024) to integrate data from all samples, followed by clustering for consistent cell type identification using the original samples' metadata and cell type markers in the three original studies.

Human Skeletal Muscle Atlas data: The data were obtained from https://www.muscleageingcellatlas.org/ and they were collected by Kedlian *et al*. (Kedlian et al. 2024). We used only the "Fibroblasts and Schwann cells" dataset, which was converted from an h5ad object to a Seurat object in R using the anndata (github.com/dynverse/anndata) and sceasy (github.com/cellgeni/sceasy) R pacakges. This data was derived from the intercostal muscles of 12 (four females, eight males) deceased donors between the ages of 15 and 75 years-old. The data was already preprocessed using SCANPY (Wolf et al. 2018), where the authors first used CellBender (Fleming et al. 2023), which removes potential technical artificats from sc/snRNA-seq data. They then filtered for cells/nuclei with mitochondrial gene expression < 10% for scRNA-seq data and <5% for snRNA-seq data, along with other gene detection and counts filters, such as a count range between 400 and 400,00. The authors also shared their cell type annotations, including non-myelinating and myelinating glia and the corresponding markers (Kedlian et al. 2024).

Cardiomyopathy heart snRNA-seq data: These data were obtained from a previous study by Reichart *et al*. The samples were collected from donor ventricles to characterize the cell type and gene program changes that occur in hearts with arrhythmogenic right ventricular and dilated cardiomyopatheis (Reichart et al. 2022). Data for 18 controls and 61 cardiomyopathy hearts were downloaded from https://cellxgene.cziscience.com/collections/e75342a8-0f3b-4ec5-8ee1-245a23e0f7cb/private. They were uploaded by the authors and processed after filtering for counts between 300 and 15,000, 300 – 5,000 detected genes for gene detection, and < 1% mitochondrial expression. Cell type annotation was also provided. Because there were no male

cells in the non-compaction cardiomyopathy samples, we eliminated this group from our analysis, leaving us with normal, arrhythmogenic right ventricular cardiomyopathy, and dilated cardiomyopathy groups.

Mouse snRNA-seq data: These data were from multiple peripheral nerves (GSE182098; snRNA-seq) (Yim et al. 2022) and sciatic nerves (GSE137870; scRNA-seq) (Gerber et al. 2021) and available as processed Seurat objects. The data by Yim *et al*. came from a combination of sciatic, sural, vagus, and peroneal nerve collections (Yim et al. 2022). For both datasets, multiple mice, regardless of sex, were pooled. Both provided detailed assessments of glial cell types/subtypes. For Yim et al. data, we used their processed data and cell type annotations without further filtering. For Gerber et al., we subclustered their labeled Schwann cells to help us differntiate myelinating from non-myelinating cells. For the data by Gerber *et al*., they were preprocessed by filtering for cells with 500 - 5000 genes, while Yim *et al*. removed nuclei with < 500 genes and with > 5% mitochondrial gene expression.

Mouse and Human Cell Atlas: The tissue and cell-type level expression data for *XIST/Xist* were obtained using the CELLxGENE Discover Gene Expression tool (CZI Cell Science Program et al. 2024). We summarize all cell-type-tissue combinations with *XIST/Xist* detection in > 30% of male cells in **Supplemental Figure S3** and provide the percentages for all other cell types by sex and tissues in **Supplemental Tables S3** and **S10**. These data came from many sources and studies, but were re-processed consistently by the CELLxGENE team, including removal of duplicate cells, cells with < 500 genes, and keeping only data derived from sequencing assays that do not require gene-length normalization, such as 10x 3’ and 5’ kits, Drop-Seq, Seq-Well, and CEL-Seq. The data can be obtained from https://cellxgene.cziscience.com/gene-expression.

Multiomic heart data: 10X multiomic scRNA/ATAC-seq data was also obtained from the Heart Cell Atlas (Kanemaru et al. 2023). ATAC fragments and peaks from ten (four female, six male) adult hearts (between 20 and 75 years-old) were obtained from https://www.heartcellatlas.org/. Author-provided metadata was used for labeling major cell types and sex. We used the Signac R package (Stuart et al. 2021) and followed the standard analysis procedures to merge data for each of the samples. Peaks were originally called based on high resolution cell types that the authors annotated. We thus utilized MACS2 (Zhang et al. 2008) to re-call peaks after merging data to the

level of broad cell types. We also analyzed the expression data after retaining only cells present in the ATAC dataset based on barcode. We then used Signac's built-in plotting functions to create ATAC coverage plots over the *XIST* locus.

CATlas data: The Cis-element Atlas (CATlas) (Zhang et al. 2021) is a crowdsourcing resource that curates human and mouse *cis*-regulatory element reference maps. We downloaded and used bigWig files without further processing. We obtained these cell-type level bigWig files for snRNA and ATAC-seq data from their curated heart and multi-tissue datasets.

sc/snRNA-seq data cell type identification

For sc/snRNA-seq data without cell type annotations for direct usage, we first computed cell type markers using Seurat's FindAllMarkers function, which performs a Wilcoxon Rank-Sum Test between cells in each cluster and all other cells. We then compared the top markers with known glia, myelination, and neuronal markers, adapted from Kanemaru et al. (Kanemaru et al. 2023), to further identify glial subtypes (myelinating, non-myelinating, or other) and to ensure that they were negative for neuronal markers. *SCN7A* was identified as a Schwann cell marker in the Human Protein Atlas (Karlsson et al.) (Karlsson et al. 2021) and is more highly expressed in non-myelinating Schwann cells by Yim et al. (Yim et al. 2022), along with *SLC35F1*. Thus, these genes were included as Schwann cell markers. *NRXN1*, *NRXN2*, *NCAM2*, *ALDH1A1*, and *S100B*, like by Kanemaru et al., were used as glial cell markers. Kanemaru et al. considered *MBP*, *MPZ*, and *PRX* as general Schwann cell markers; however, we used these myelinating genes in addition to *PLP1*, which encodes a major component of myelin (Diehl et al. 1986), to specifically identify myelinating Schwann cells. We also added *XIST*, *CADM2*, and *SMYD3*, which were markers for cardiac non-myelinating Schwann cells from our integrated data. *NGF* was used to identify "other" glia since *NGF*+ heart glia clustered separately. Because *NRXN1* and *NRXN2* are also expressed in neurons, we needed to include genes to ensure that glia were not neurons. For this, we used the same neuronal markers as Kanemaru *et al*., which included *PRPH*, *STMN2*, *CACNA1B*, *NEFL*, *NEFM*, *NEFH*, *DLG4*, and *TUBB3*. The markers listed here were also used to identify Schwann cells in non-heart datasets when such cell types were not defined or shared by the original authors.

Differential expression analysis

For sc/snRNA-seq datasets, pseudobulking by cell type or subcluster was performed prior to differential expression analysis with DESeq2 (Love et al. 2014) in order to use the sample replicates appropriately. For the integrated human heart data, a group variable was introduced to account for batch effects (e.g., labs) observed across datasets. All other parameters were set to default. For more information on density plots, gene set enrichment analysis, and overrepresentation analysis, please refer to **Supplemental Methods**.

Defining genes with strong expression correlation with sXIST

To predict genes that may be regulated by the *sXIST* transcript, we applied co-expression analysis to the human peripheral nerve bulk RNA-seq data from Sandy-Hindmarch *et al*. To control for the effect of expression level, we first needed to obtain a list of genes with similar levels of expression as *XIST*. Based on the DESeq2-normalized count data, we filtered for genes with mean expression values across samples within +/- 3 of *XIST*'s mean. After, we randomly selected 100 of such genes and calculated the Pearson's correlation between them (and *XIST*) and all other genes across male and female samples, separately. Thus, for each of these 101 genes, we obtained male and female correlation coefficient values with the rest of the (expressing) human genes. The values were used to prepare a female vs male correlation coefficient 2D plot. We next fit an ellipse around 99% of the data points to obtain a background null distribution. Applying this ellipse to the correlation coefficients for *XIST,* we obtained genes whose expression correlation with *XIST* were higher than the null background, i.e., outliers located outside of the ellipse. We further filtered for genes with an absolute difference > 0.3 between their correlation coefficients in male and female samples and grouped them into two groups: Stronger Negative Correlation (SNC) genes (male correlation coefficient (r) < 0 and p-value < 0.05), and Stronger Positive Correlation (SPC) genes (male correlation coefficient (r) > 0 and *p*-value < 0.05).

Pooled mouse scRNA-seq sex prediction

To predict each cell's sex (XX/XY) for pooled mouse sc/snRNA-seq samples, we first obtained a list of all Y Chromosome genes using the biomaRt (Durinck et al. 2009) R package. We then annotated a cell as male if it showed expression of any of the Y Chromosome genes. Changing this to stricter criterion, e.g., increasing the expression counts to 3, did not affect our results. For

the mixed peripheral nerve data by Yim *et al*., we eliminated Y Chromosome genes starting with "Gm" from this filtering step, which were abundant in the dataset (perhaps due to their abundance in snRNA-seq). To assess the positive rate of this cell-level sex prediction, we used integrated heart and the Skeletal Muscle Atlas single cell/nucleus data, described above.

Data Access

RNA-seq data from HEK-293T cells were deposited to the GEO database (accession number GSE309419). All analysis codes in R (R Core Team 2023) are publicly available at https://github.com/bioinfoDZ/sXIST and included in **Supplemental Codes**.

Conflict of Interest: none declared.

Acknowledgements

The authors would like to thank the Einstein High Performance Computing and members in the Zheng Lab for providing valuable suggestions. This study was supported partially by the National Heart, Lung, and Blood Institute (NHLBI) grants R01HL153920 and R01HL163667 (B.M., D.Z) and by the National Institute of Arthritis and Musculoskeletal and Skin Diseases (NIAMS) grants R01AR069078 and P30AR079200 (E.E).

Author contributions

K.O. and D.Z. conceived and designed the study. K.O. performed all the bioinformatics data analysis, with assistance from K.J. M.L. and E.E. performed the *sXIST* overexpression assay. L.S. and B.M. contributed to the mouse data analysis. K.O. and D.Z. wrote the manuscript. All authors reviewed and edited the manuscript.

References

Almalki WH. 2024. Unraveling the role of Xist RNA in cardiovascular pathogenesis. *Pathology - Research and Practice* **253**: 154944.

Borsani G, Tonlorenzi R, Simmler MC, Dandolo L, Arnaud D, Capra V, Grompe M, Pizzuti A, Muzny D, Lawrence C et al. 1991. Characterization of a murine gene expressed from the inactive X chromosome. *Nature* **351**: 325-329.

Brockdorff N. 2002. X-chromosome inactivation: closing in on proteins that bind Xist RNA. *Trends in Genetics* **18**: 352-358.

Brockdorff N, Ashworth A, Kay GF, Cooper P, Smith S, McCabe VM, Norris DP, Penny GD, Patel D, Rastan S. 1991. Conservation of position and exclusive expression of mouse Xist from the inactive X chromosome. *Nature* **351**: 329-331.

Brown CJ, Ballabio A, Rupert JL, Lafreniere RG, Grompe M, Tonlorenzi R, Willard HF. 1991. A gene from the region of the human X inactivation centre is expressed exclusively from the inactive X chromosome. *Nature* **349**: 38-44.

Cerase A, Pintacuda G, Tattermusch A, Avner P. 2015. Xist localization and function: new insights from multiple levels. *Genome Biology* **16**: 166.

Chen J, Bardes EE, Aronow BJ, Jegga AG. 2009. ToppGene Suite for gene list enrichment analysis and candidate gene prioritization. *Nucleic Acids Res* **37**: W305-311.

Chen Y, Wang X. 2020. miRDB: an online database for prediction of functional microRNA targets. *Nucleic Acids Research* **48**: D127-D131.

Cheng X, Xu J, Yu Z, Xu J, Long H. 2020. LncRNA Xist Contributes to Endogenous Neurological Repair After Chronic Compressive Spinal Cord Injury by Promoting Angiogenesis Through the miR-32-5p/Notch-1 Axis. *Frontiers in Cell and Developmental Biology* **8**.

Connell M, Chen H, Jiang J, Kuan CW, Fotovati A, Chu TL, He Z, Lengyell TC, Li H, Kroll T et al. 2017. HMMR acts in the PLK1-dependent spindle positioning pathway and supports neural development. *Elife* **6**.

Coolen M, Katz S, Bally-Cuif L. 2013. miR-9: a versatile regulator of neurogenesis. *Front Cell Neurosci* **7**: 220.

CZI Cell Science Program, Abdulla S, Aevermann B, Assis P, Badajoz S, Bell SM, Bezzi E, Cakir B, Chaffer J, Chambers S et al. 2024. CZ CELLxGENE Discover: a single-cell data platform for scalable exploration, analysis and modeling of aggregated data. *Nucleic Acids Research* **53**: D886–D900.

Danecek P, Bonfield JK, Liddle J, Marshall J, Ohan V, Pollard MO, Whitwham A, Keane T, McCarthy SA, Davies RM et al. 2021. Twelve years of SAMtools and BCFtools. *GigaScience* **10**: giab008.

Dantas TJ. 2020. Centrosomes and cilia: always at the center of the action. *Communications Biology* **3**: 785.

Diehl HJ, Schaich M, Budzinski RM, Stoffel W. 1986. Individual exons encode the integral membrane domains of human myelin proteolipid protein. *Proc Natl Acad Sci U S A* **83**: 9807-9811.

Dobin A, Davis CA, Schlesinger F, Drenkow J, Zaleski C, Jha S, Batut P, Chaisson M, Gingeras TR. 2013. STAR: ultrafast universal RNA-seq aligner. *Bioinformatics* **29**: 15-21.

Dror I, Chitiashvili T, Tan SYX, Cano CT, Sahakyan A, Markaki Y, Chronis C, Collier AJ, Deng W, Liang G et al. 2024. XIST directly regulates X-linked and autosomal genes in naive human pluripotent cells. *Cell* **187**: 110-129.e131.

Durinck S, Spellman PT, Birney E, Huber W. 2009. Mapping identifiers for the integration of genomic datasets with the R/Bioconductor package biomaRt. *Nature Protocols* **4**: 1184-1191.

Fleming SJ, Chaffin MD, Arduini A, Akkad A-D, Banks E, Marioni JC, Philippakis AA, Ellinor PT, Babadi M. 2023. Unsupervised removal of systematic background noise from droplet-based single-cell experiments using CellBender. *Nature Methods* **20**: 1323-1335.

Gerber D, Pereira JA, Gerber J, Tan G, Dimitrieva S, Yángüez E, Suter U. 2021. Transcriptional profiling of mouse peripheral nerves to the single-cell level to build a sciatic nerve ATlas (SNAT). *eLife* **10**: e58591.

Gorin G, Goodman L. 2025. Male XIST expression in cardiac pseudo-glia does not induce X chromosome inactivation. *bioRxiv* doi:10.1101/2025.04.09.648005: 2025.2004.2009.648005.

Hao Y, Stuart T, Kowalski MH, Choudhary S, Hoffman P, Hartman A, Srivastava A, Molla G, Madad S, Fernandez-Granda C et al. 2024. Dictionary learning for integrative, multimodal and scalable single-cell analysis. *Nat Biotechnol* **42**: 293-304.

Hausser J, Zavolan M. 2014. Identification and consequences of miRNA–target interactions — beyond repression of gene expression. *Nature Reviews Genetics* **15**: 599-612.

Helena Mangs A, Morris BJ. 2007. The Human Pseudoautosomal Region (PAR): Origin, Function and Future. *Curr Genomics* **8**: 129-136.

Heming M, Börsch A-L, Wolbert J, Thomas C, Mausberg AK, Szepanowski F, Eggert B, Lu IN, Tietz J, Dienhart F et al. 2025. Multi-omic identification of perineurial hyperplasia and lipid-associated nerve macrophages in human polyneuropathies. *Nature Communications* **16**: 7872.

Hortells L, Meyer EC, Thomas ZM, Yutzey KE. 2021. Periostin-expressing Schwann cells and endoneurial cardiac fibroblasts contribute to sympathetic nerve fasciculation after birth. *J Mol Cell Cardiol* **154**: 124-136.

Jacobson EC, Pandya-Jones A, Plath K. 2022. A lifelong duty: how Xist maintains the inactive X chromosome. *Current Opinion in Genetics & Development* **75**: 101927.

Jiang R, Zhang H, Zhou J, Wang J, Xu Y, Zhang H, Gu Y, Fu F, Shen Y, Zhang G et al. 2021. Inhibition of long non-coding RNA XIST upregulates microRNA-149-3p to repress ovarian cancer cell progression. *Cell Death & Disease* **12**: 145.

Johnston CM, Nesterova TB, Formstone EJ, Newall AE, Duthie SM, Sheardown SA, Brockdorff N. 1998. Developmentally regulated Xist promoter switch mediates initiation of X inactivation. *Cell* **94**: 809-817.

Kanemaru K, Cranley J, Muraro D, Miranda AMA, Ho SY, Wilbrey-Clark A, Patrick Pett J, Polanski K, Richardson L, Litvinukova M et al. 2023. Spatially resolved multiomics of human cardiac niches. *Nature* **619**: 801-810.

Karlsson M, Zhang C, Méar L, Zhong W, Digre A, Katona B, Sjöstedt E, Butler L, Odeberg J, Dusart P et al. 2021. A single–cell type transcriptomics map of human tissues. *Science Advances* **7**: eabh2169.

Kavakiotis I, Alexiou A, Tastsoglou S, Vlachos Ioannis S, Hatzigeorgiou Artemis G. 2022. DIANA-miTED: a microRNA tissue expression database. *Nucleic Acids Research* **50**: D1055-D1061.

Kedlian VR, Wang Y, Liu T, Chen X, Bolt L, Tudor C, Shen Z, Fasouli ES, Prigmore E, Kleshchevnikov V et al. 2024. Human skeletal muscle aging atlas. *Nature Aging* **4**: 727-744.

Ki SM, Jeong HS, Lee JE. 2021. Primary Cilia in Glial Cells: An Oasis in the Journey to Overcoming Neurodegenerative Diseases. *Front Neurosci* **15**: 736888.

Leung AKL. 2015. The Whereabouts of microRNA Actions: Cytoplasm and Beyond. *Trends Cell Biol* **25**: 601-610.

Li B, Dewey CN. 2011. RSEM: accurate transcript quantification from RNA-Seq data with or without a reference genome. *BMC Bioinformatics* **12**: 323.

Li C, Wan L, Liu Z, Xu G, Wang S, Su Z, Zhang Y, Zhang C, Liu X, Lei Z et al. 2018. Long non-coding RNA XIST promotes TGF-β-induced epithelial-mesenchymal transition by

regulating miR-367/141-ZEB2 axis in non-small-cell lung cancer. *Cancer Letters* **418**: 185-195.

Liu H, Deng H, Zhao Y, Li C, Liang Y. 2018. LncRNA XIST/miR-34a axis modulates the cell proliferation and tumor growth of thyroid cancer through MET-PI3K-AKT signaling. *J Exp Clin Cancer Res* **37**: 279.

Liu T-T, Li R, Liu X, Zhou X-J, Huo C, Li J-P, Qu Y-Q. 2021. LncRNA XIST acts as a MicroRNA-520 sponge to regulate the Cisplatin resistance in NSCLC cells by mediating BAX through CeRNA network. *International Journal of Medical Sciences* **18**: 419-431.

Loda A, Heard E. 2019. Xist RNA in action: Past, present, and future. *PLoS Genet* **15**: e1008333.

Loges NT, Olbrich H, Becker-Heck A, Häffner K, Heer A, Reinhard C, Schmidts M, Kispert A, Zariwala MA, Leigh MW et al. 2009. Deletions and Point Mutations of LRRC50 Cause Primary Ciliary Dyskinesia Due to Dynein Arm Defects. *The American Journal of Human Genetics* **85**: 883-889.

Lonsdale J Thomas J Salvatore M Phillips R Lo E Shad S Hasz R Walters G Garcia F Young N et al. 2013. The Genotype-Tissue Expression (GTEx) project. *Nature Genetics* **45**: 580-585.

Looijenga LH, Gillis AJ, van Gurp RJ, Verkerk AJ, Oosterhuis JW. 1997. X inactivation in human testicular tumors. XIST expression and androgen receptor methylation status. *Am J Pathol* **151**: 581-590.

Love MI, Huber W, Anders S. 2014. Moderated estimation of fold change and dispersion for RNA-seq data with DESeq2. *Genome Biology* **15**: 550.

Luo Y, Hitz BC, Gabdank I, Hilton JA, Kagda MS, Lam B, Myers Z, Sud P, Jou J, Lin K et al. 2020. New developments on the Encyclopedia of DNA Elements (ENCODE) data portal. *Nucleic Acids Res* **48**: D882-d889.

Marshall EA, Stewart GL, Sage AP, Lam WL, Brown CJ. 2019. Beyond sequence homology: Cellular biology limits the potential of XIST to act as a miRNA sponge. *PLoS One* **14**: e0221371.

Mattick JS, Amaral PP, Carninci P, Carpenter S, Chang HY, Chen LL, Chen R, Dean C, Dinger ME, Fitzgerald KA et al. 2023. Long non-coding RNAs: definitions, functions, challenges and recommendations. *Nat Rev Mol Cell Biol* **24**: 430-447.

McCarrey JR, Watson C, Atencio J, Ostermeier GC, Marahrens Y, Jaenisch R, Krawetz SA. 2002. X-chromosome inactivation during spermatogenesis is regulated by an Xist/Tsix-independent mechanism in the mouse. *Genesis* **34**: 257-266.

1020 Mehdiabadi NR, Boon Sim C, Phipson B, Kalathur RKR, Sun Y, Vivien CJ, Ter Huurne M, Piers
1021 AT, Hudson JE, Oshlack A et al. 2022. Defining the Fetal Gene Program at Single-Cell
1022 Resolution in Pediatric Dilated Cardiomyopathy. *Circulation* **146**: 1105-1108.

1023 Memili E, Hong Y-K, Kim D-H, Ontiveros SD, Strauss WM. 2001. Murine Xist RNA isoforms
1024 are different at their 3′ ends: a role for differential polyadenylation. *Gene* **266**: 131-137.

1025 Miao C, Jiang Q, Li H, Zhang Q, Bai B, Bao Y, Zhang T. 2016. Mutations in the Motile Cilia
1026 Gene DNAAF1 Are Associated with Neural Tube Defects in Humans. *G3*
1027 *Genes|Genomes|Genetics* **6**: 3307-3316.

1028 Morey C, Rougeulle C, Ouimette J-F. 2025. Unleashing XIST from X-chromosome inactivation.
1029 *Current Opinion in Cell Biology* **92**: 102446.

1030 Mudge JM, Carbonell-Sala S, Diekhans M, Martinez JG, Hunt T, Jungreis I, Loveland JE, Arnan
1031 C, Barnes I, Bennett R et al. 2025. GENCODE 2025: reference gene annotation for
1032 human and mouse. *Nucleic Acids Res* **53**: D966-d975.

1033 Noguchi S Arakawa T Fukuda S Furuno M Hasegawa A Hori F Ishikawa-Kato S Kaida K Kaiho
1034 A Kanamori-Katayama M et al. 2017. FANTOM5 CAGE profiles of human and mouse
1035 samples. *Scientific Data* **4**: 170112.

1036 Ouasti S, Faroni A, Kingham PJ, Ghibaudi M, Reid AJ, Tirelli N. 2020. Hyaluronic Acid (HA)
1037 Receptors and the Motility of Schwann Cell(-Like) Phenotypes. *Cells* **9**.

1038 Panning B. 2008. X-chromosome inactivation: the molecular basis of silencing. *Journal of*
1039 *Biology* **7**: 30.

1040 Perez G, Barber GP, Benet-Pages A, Casper J, Clawson H, Diekhans M, Fischer C, Gonzalez JN,
1041 Hinrichs AS, Lee CM et al. 2025. The UCSC Genome Browser database: 2025 update.
1042 *Nucleic Acids Res* **53**: D1243-d1249.

1043 Politz JC, Zhang F, Pederson T. 2006. MicroRNA-206 colocalizes with ribosome-rich regions in
1044 both the nucleolus and cytoplasm of rat myogenic cells. *Proc Natl Acad Sci U S A* **103**:
1045 18957-18962.

1046 R Core Team. 2023. R: A Language and Environment for Statistical Computing.

1047 Rauluseviciute I, Riudavets-Puig R, Blanc-Mathieu R, Castro-Mondragon Jaime A, Ferenc K,
1048 Kumar V, Lemma RB, Lucas J, Chèneby J, Baranasic D et al. 2024. JASPAR 2024: 20th
1049 anniversary of the open-access database of transcription factor binding profiles. *Nucleic*
1050 *Acids Research* **52**: D174-D182.

Reichart D, Lindberg EL, Maatz H, Miranda AMA, Viveiros A, Shvetsov N, Gärtner A, Nadelmann ER, Lee M, Kanemaru K et al. 2022. Pathogenic variants damage cell composition and single cell transcription in cardiomyopathies. *Science* **377**: eabo1984.

Rishik S, Hirsch P, Grandke F, Fehlmann T, Keller A. 2025. miRNATissueAtlas 2025: an update to the uniformly processed and annotated human and mouse non-coding RNA tissue atlas. *Nucleic Acids Research* **53**: D129-D137.

Robinson JT, Thorvaldsdóttir H, Winckler W, Guttman M, Lander ES, Getz G, Mesirov JP. 2011. Integrative genomics viewer. *Nature Biotechnology* **29**: 24-26.

Sadagopan A, Nasim IT, Li J, Achom M, Zhang C-Z, Viswanathan SR. 2022. Somatic XIST activation and features of X chromosome inactivation in male human cancers. *Cell Systems* **13**: 932-944.e935.

Salido EC, Yen PH, Mohandas TK, Shapiro LJ. 1992. Expression of the X-inactivation-associated gene XIST during spermatogenesis. *Nat Genet* **2**: 196-199.

Sandy-Hindmarch OP, Chang P-S, Scheuren PS, De Schoenmacker I, Hubli M, Loizou C, Wirth S, Mahadevan D, Wiberg A, Furniss D et al. 2025. The local molecular signature of human peripheral neuropathic pain. *PAIN* **166**: 1143-1156.

Sim CB, Phipson B, Ziemann M, Rafehi H, Mills RJ, Watt KI, Abu-Bonsrah KD, Kalathur RKR, Voges HK, Dinh DT et al. 2021. Sex-Specific Control of Human Heart Maturation by the Progesterone Receptor. *Circulation* **143**: 1614-1628.

Sleiman Y, Lacampagne A, Meli AC. 2021. “Ryanopathies” and RyR2 dysfunctions: can we further decipher them using in vitro human disease models? *Cell Death & Disease* **12**: 1041.

Spezzacatene A, Sinagra G, Merlo M, Barbati G, Graw SL, Brun F, Slavov D, Di Lenarda A, Salcedo EE, Towbin JA et al. 2015. Arrhythmogenic Phenotype in Dilated Cardiomyopathy: Natural History and Predictors of Life-Threatening Arrhythmias. *J Am Heart Assoc* **4**: e002149.

Statello L, Guo CJ, Chen LL, Huarte M. 2021. Gene regulation by long non-coding RNAs and its biological functions. *Nat Rev Mol Cell Biol* **22**: 96-118.

Stuart T, Srivastava A, Madad S, Lareau CA, Satija R. 2021. Single-cell chromatin state analysis with Signac. *Nature Methods* **18**: 1333-1341.

Sunwoo H, Colognori D, Froberg JE, Jeon Y, Lee JT. 2017. Repeat E anchors Xist RNA to the inactive X chromosomal compartment through CDKN1A-interacting protein (CIZ1). *Proceedings of the National Academy of Sciences* **114**: 10654-10659.

The ENCODE Project Consortium. 2012. An integrated encyclopedia of DNA elements in the human genome. *Nature* **489**: 57-74.

Tukiainen T Villani A-C Yen A Rivas MA Marshall JL Satija R Aguirre M Gauthier L Fleharty M Kirby A et al. 2017. Landscape of X chromosome inactivation across human tissues. *Nature* **550**: 244-248.

Turunen TA, Roberts TC, Laitinen P, Väänänen M-A, Korhonen P, Malm T, Ylä-Herttuala S, Turunen MP. 2019. Changes in nuclear and cytoplasmic microRNA distribution in response to hypoxic stress. *Scientific Reports* **9**: 10332.

Twa GM, Phillips RA, Robinson NJ, Day JJ. 2024. Accurate sample deconvolution of pooled snRNA-seq using sex-dependent gene expression patterns. *bioRxiv* doi:10.1101/2024.11.29.626066: 2024.2011.2029.626066.

Velmeshev D, Schirmer L, Jung D, Haeussler M, Perez Y, Mayer S, Bhaduri A, Goyal N, Rowitch DH, Kriegstein AR. 2019. Single-cell genomics identifies cell type-specific molecular changes in autism. *Science* **364**: 685-689.

Wainer Katsir K, Linial M. 2019. Human genes escaping X-inactivation revealed by single cell expression data. *BMC Genomics* **20**: 201.

Wamsley B, Bicks L, Cheng Y, Kawaguchi R, Quintero D, Margolis M, Grundman J, Liu J, Xiao S, Hawken N et al. 2024. Molecular cascades and cell type–specific signatures in ASD revealed by single-cell genomics. *Science* **384**: eadh2602.

Wang H, Li Y, Jiang S, Liu N, Zhou Q, Li Q, Chen Z, Lin Y, Chen C, Deng Y. 2023. LncRNA xist regulates sepsis associated neuroinflammation in the periventricular white matter of CLP rats by miR-122-5p/PKCη Axis. *Front Immunol* **14**: 1225482.

Weng S, Stoner SA, Zhang DE. 2016. Sex chromosome loss and the pseudoautosomal region genes in hematological malignancies. *Oncotarget* **7**: 72356-72372.

Wolf FA, Angerer P, Theis FJ. 2018. SCANPY: large-scale single-cell gene expression data analysis. *Genome Biology* **19**: 15.

Wolock SL, Lopez R, Klein AM. 2019. Scrublet: Computational Identification of Cell Doublets in Single-Cell Transcriptomic Data. *Cell Syst* **8**: 281-291.e289.

Wu W, Ji P, Zhao F. 2020. CircAtlas: an integrated resource of one million highly accurate circular RNAs from 1070 vertebrate transcriptomes. *Genome Biology* **21**: 101.

Yan Z, Li J, Guo J, He R, Xing J. 2022. LncRNA XIST sponges microRNA-448 to promote malignant behaviors of colorectal cancer cells via regulating GRHL2. *Functional & Integrative Genomics* **22**: 977-988.

Yang LL, Li Q, Zhang X, Cao T. 2020. Long non-coding RNA XIST confers aggressive progression via miR-361-3p/STX17 in retinoblastoma cells. *Eur Rev Med Pharmacol Sci* **24**: 10433-10444.

Yao S, Jeon Y, Kesner B, Lee JT. 2024. Xist RNA binds select autosomal genes and depends on Repeat B to regulate their expression. **13**: RP101197.

Yim AKY, Wang PL, Bermingham JR, Jr., Hackett A, Strickland A, Miller TM, Ly C, Mitra RD, Milbrandt J. 2022. Disentangling glial diversity in peripheral nerves at single-nuclei resolution. *Nat Neurosci* **25**: 238-251.

Yue M, Ogawa Y. 2018. CRISPR/Cas9-mediated modulation of splicing efficiency reveals short splicing isoform of Xist RNA is sufficient to induce X-chromosome inactivation. *Nucleic Acids Res* **46**: e26.

Zhang K, Hocker JD, Miller M, Hou X, Chiou J, Poirion OB, Qiu Y, Li YE, Gaulton KJ, Wang A et al. 2021. A single-cell atlas of chromatin accessibility in the human genome. *Cell* **184**: 5985-6001.e5919.

Zhang Y, Liu T, Meyer CA, Eeckhoute J, Johnson DS, Bernstein BE, Nusbaum C, Myers RM, Brown M, Li W et al. 2008. Model-based Analysis of ChIP-Seq (MACS). *Genome Biology* **9**: R137.

Zheng C, Bai C, Sun Q, Zhang F, Yu Q, Zhao X, Kang S, Li J, Jia Y. 2020. Long noncoding RNA XIST regulates osteogenic differentiation of human bone marrow mesenchymal stem cells by targeting miR-9-5p. *Mech Dev* **162**: 103612.

Zhou S, Gao R, Hu W, Qian T, Wang N, Ding G, Ding F, Yu B, Gu X. 2014. MiR-9 inhibits Schwann cell migration by targeting Cthrc1 following sciatic nerve injury. *J Cell Sci* **127**: 967-976.

Figure Legends:

Figure 1: High *XIST* expression in non-myelinating Schwann cells from male human heart and skeletal muscle tissue. A) Clusters of 510,171 human heart cells from 11 male and 9 female individuals. Cells within the dashed box are glia, which are colored by subtypes. EC, endothelial cells; FB, fibroblasts; aCM, atrial cardiomyocytes; vCM, ventricular cardiomyocytes;

mSchwann, myelinating Schwann; nmSchwann, non-myelinating Schwann. **B/E)** A variety of positive and negative markers used to identify male and female myelinating and non-myelinating Schwann cells. **C/F)** Seurat-normalized *XIST* expression across all cells, grouped by cell types and split by sexes. The asterisk represents a significant difference in expression between male non-myelinating (nm) and myelinating (m) Schwann cells. **D)** Clusters of 20,611 skeletal muscle fibroblast and neural cells from 8 male and 4 female individuals, colored by cell annotations provided by the original authors.

Figure 2: Chromatin accessibility at the *XIST* locus across human heart cell types. A) Multiomic scATAC/RNA-seq signal and expression (split by sex) across cell types. MACS2-called peaks are represented as "cell-type peaks." The normalized signal across all cells and fragments for 100 random cells are presented above the *XIST* gene locus, with introns and exons as thin and thick green lines, respectively. **B)** A zoomed-in view of scATAC-seq signal for male (blue) and female (brown) glia. **A-B)** The red highlighted region represents the glia-specific peak (ChrX:73,841,364-73,841,611) called by MACS2.

Figure 3: Assessment of ATAC, RNA, and ChIP-seq read coverages over the *XIST* locus. A) snRNA/ATAC-seq tracks from CATlas heart dataset. **B)** RNA-seq (+/- strands), H3K4me3, H3K4me1, H3K27ac, and H3K36me3 ChIP-seq from two human male tibial nerve samples and ATAC-seq tracks from one human male and two female sciatic nerve samples in the ENCODE database. **C)** snATAC-seq tracks from CATlas multi-tissue dataset. **A-C)** All plots show the region at ChrX:73,790,905-73,854,216 from the hg38 reference genome. The 3' region of *XIST* exon 1 is enclosed by two red dashed lines. *TSIX* gene location spanning ChrX:73,792,205-73,829,231 on the + strand is shown as a blue bar, indicating the RNA-seq reads were from *XIST* but not *TSIX*. For each track, cell types and/or sequencing modality are shown on the left while the data range is shown in the right. Additional data for the tibial and sciatic nerve samples are in **Supplemental Figure S7**.

Figure 4: Potential roles of *XIST* in peripheral nerve. A-B) Density plots of $\log_2$FC from a variety of gene group comparisons using human skeletal muscle data (**A**) and human heart data **(B)** along with their expected and observed trends. For X Chromosome non-escapee genes, the expected trend is based on the presumption that *sXIST* participates in XCI. In all comparisons, the $\log_2$FC values were computed from $\log_2$(sample-on-right/sample-on-left). Gene groups with too few genes for robust density analysis in a comparison were not included in these plots. Expected and observed trends for **A** and **B** are summarized at the bottom. **C)** Pearson correlation coefficients (r) between *XIST* and all other genes computed separately for males (x-axis) and females (y-axis) using peripheral nerve bulk RNA-seq data. In this plot, each dot is a gene, and the predicted 99% confidence ellipse was overlayed (refer to **Supplemental Figure S12**). Outlier genes with a male Pearson's correlation *p*-value < 0.05 and absolute difference > 0.3 between male and female correlation coefficients were colored red if male r > 0 and blue if male r < 0. **D)**

Two gene examples (*DNAAF1* and *KCNAB1*) exhibiting stronger positive (red) and negative (blue) expression correlation with *XIST* in males. Expression values are provided as $\log_2$(DESeq2-normalized counts +1). **E-F**) Overrepresentation analysis for genes with stronger negative male correlations **(E)** or stronger positive male correlations **(F).** Dot size represents the number of query genes in each term and color is -log(FDR adjusted *p*-value).

Figure 5: RNA-seq analysis of *sXIST* overexpression. A) IGV tracks showing RNA-seq reads over ChrX:73,790,905-73,854,216, with *TSIX* and *XIST* indicated. Samples overexpressing the second half of exon 6 (*XIST* OE) are shown in red while GFP controls (Ctrl) are in blue. **B)** Density and boxplots showing $\log_2$FC values across gene groups. Values above boxplots are the mean $\log_2$FC for that group. **C)** Heatmap of the DEGs (adjusted *p*-values < 0.05 and |fold change| > 1.5). **D-E)** ToppFun results from downregulated (**D**) and upregulated (**E**) genes in **C**. **F)** Boxplots showing the expression of *XIST*, *DNAAF1*, and *HMMR*. **G)**. Cloned *XIST*, *DNAAF1*, and *HMMR* transcript sequence alignments with hsa-miR-9-5p.

Figure 6: *XIST* expression in arrhythmogenic and dilated cardiomyopathy. A) UMAP of 881,081 heart nuclei from snRNA-seq data performed on 61 heart failure patients and 18 healthy controls (Reichart et al. 2022). Cells originally labeled “neural” were renamed to “glia” based on expression of glial markers (**Supplemental Figure S14**). **B)** Normalized *XIST* expression across all nuclei, grouped by cell type and split by sex. For males, the percentages of cells expressing *XIST* are shown at the top. **C-I)** Cells were subset by glia cell type annotation and grouped based on arrhythmogenic (arrhyth) RV cardiomyopathy, dilated cardiomyopathy, and normal (healthy) annotations and sex. Normalized *XIST* **(C)**, *FOXO1* **(E)**, *COL4A6* **(F)**, and *RYR2* **(G)** expression after pseudobulking glial cells by donor. **D)** The percentage of glial cells that express *XIST* for each sample by disease group and sex. **H-I**) Module scoring was performed on SPC (**E**) and SNC (**I**) genes from **Figure 4**. Asterisks indicate a significant difference using Fisher’s exact test **(D)** or DESeq2 negative binomial test **(C,E-I)**.

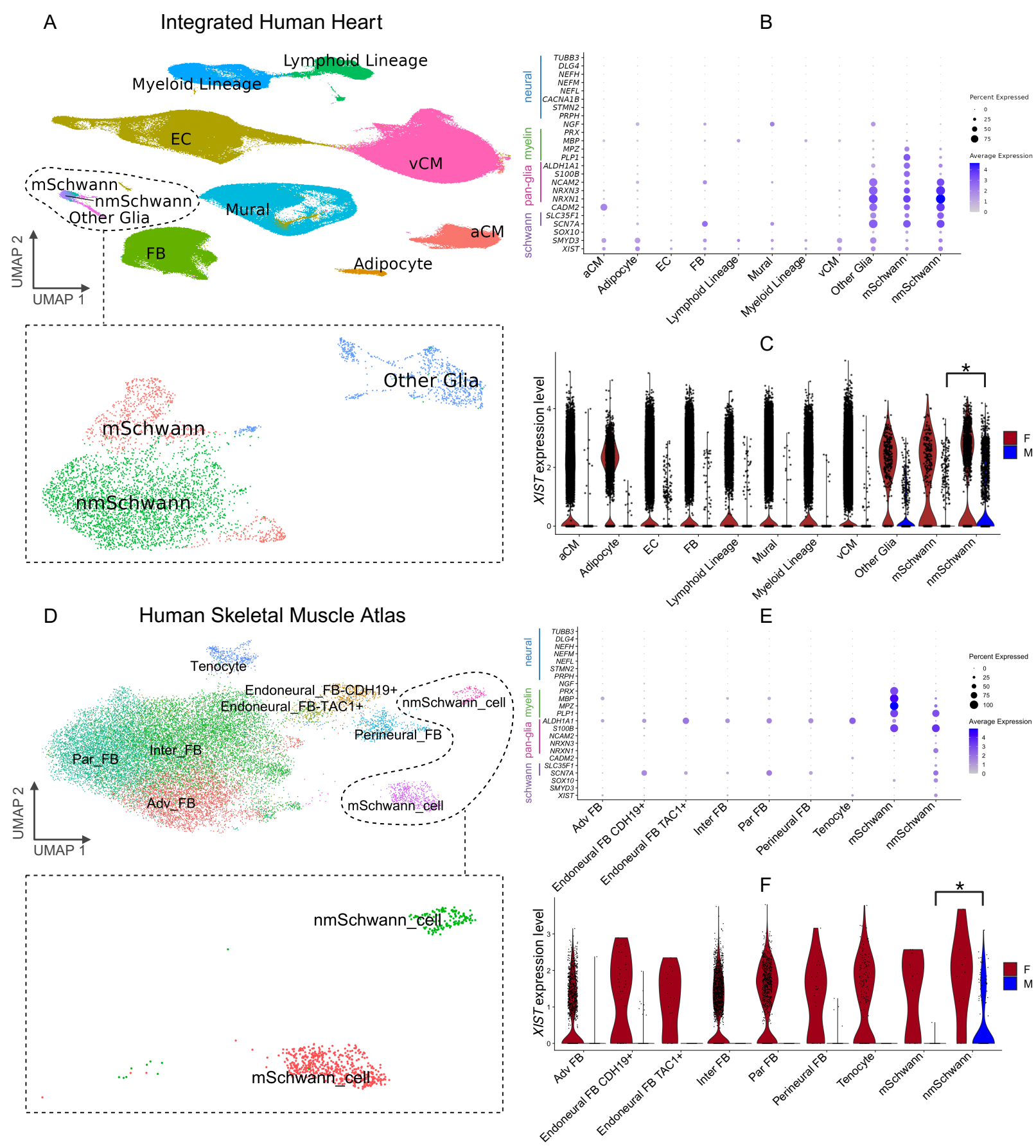
A
Integrated Human Heart
Lymphoid Lineage
Myeloid Lineage
EC
vCM
mSchwann
nmSchwann
Other Glia
Mural
aCM
FB
Adipocyte
UMAP 2
UMAP 1
Other Glia
mSchwann
nmSchwann
B
neural
myelin
pan-glia
schwann
TUBB3
DLG4
NEFH
NEFM
NEFL
CACNA1B
STMN2
PRPH
NGF
PRX
MBP
MPZ
PLP1
ALDH1A1
S100B
NCAM2
NRXN3
NRXN1
CADM2
SLC35F1
SCN7A
SOX10
SMYD3
XIST
Percent Expressed
Average Expression
aCM
Adipocyte
EC
FB
Lymphoid Lineage
Mural
Myeloid Lineage
vCM
Other Glia
mSchwann
nmSchwann
C
XIST expression level
*
F
M
D
Human Skeletal Muscle Atlas
Tenocyte
Endoneural_FB-CDH19+
Endoneural_FB-TAC1+
nmSchwann_cell
Perineural_FB
Par_FB
Inter_FB
Adv_FB
mSchwann_cell
UMAP 2
UMAP 1
nmSchwann_cell
mSchwann_cell
E
Adv FB
Endoneural FB CDH19+
Endoneural FB TAC1+
Inter FB
Par FB
Perineural FB
Tenocyte
mSchwann
nmSchwann
F
XIST expression level
*
F
M

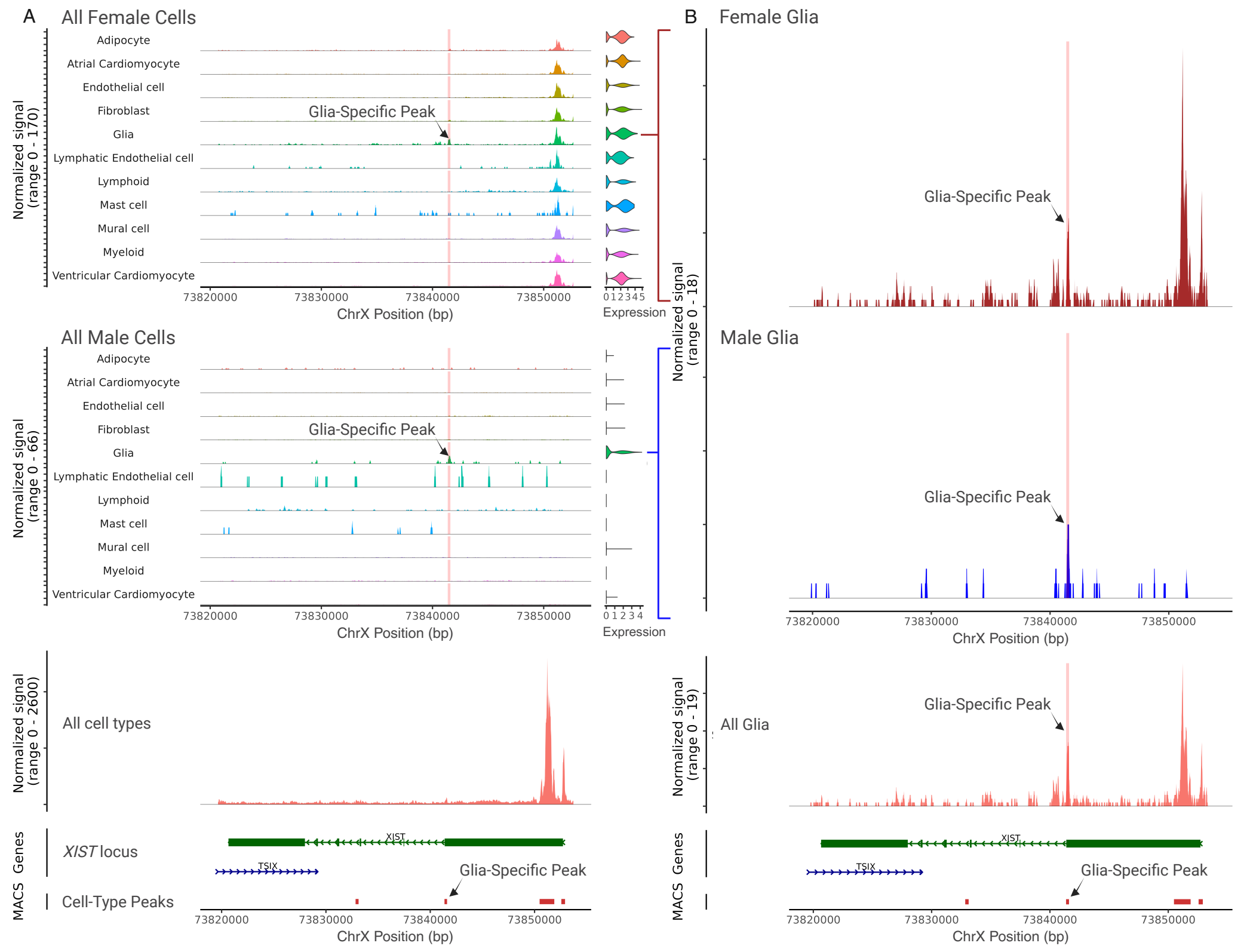
A
All Female Cells
Adipocyte
Atrial Cardiomyocyte
Endothelial cell
Fibroblast
Glia
Lymphatic Endothelial cell
Lymphoid
Mast cell
Mural cell
Myeloid
Ventricular Cardiomyocyte
Glia-Specific Peak
Normalized signal (range 0 - 170)
73820000
73830000
73840000
73850000
ChrX Position (bp)
0 1 2 3 4 5
Expression
All Male Cells
Glia-Specific Peak
Normalized signal (range 0 - 66)
0 1 2 3 4
B
Female Glia
Glia-Specific Peak
Normalized signal (range 0 - 18)
Male Glia
Glia-Specific Peak
All cell types
Normalized signal (range 0 - 2600)
All Glia
Normalized signal (range 0 - 19)
Genes
XIST
TSIX
XIST locus
MACS
Cell-Type Peaks
Glia-Specific Peak

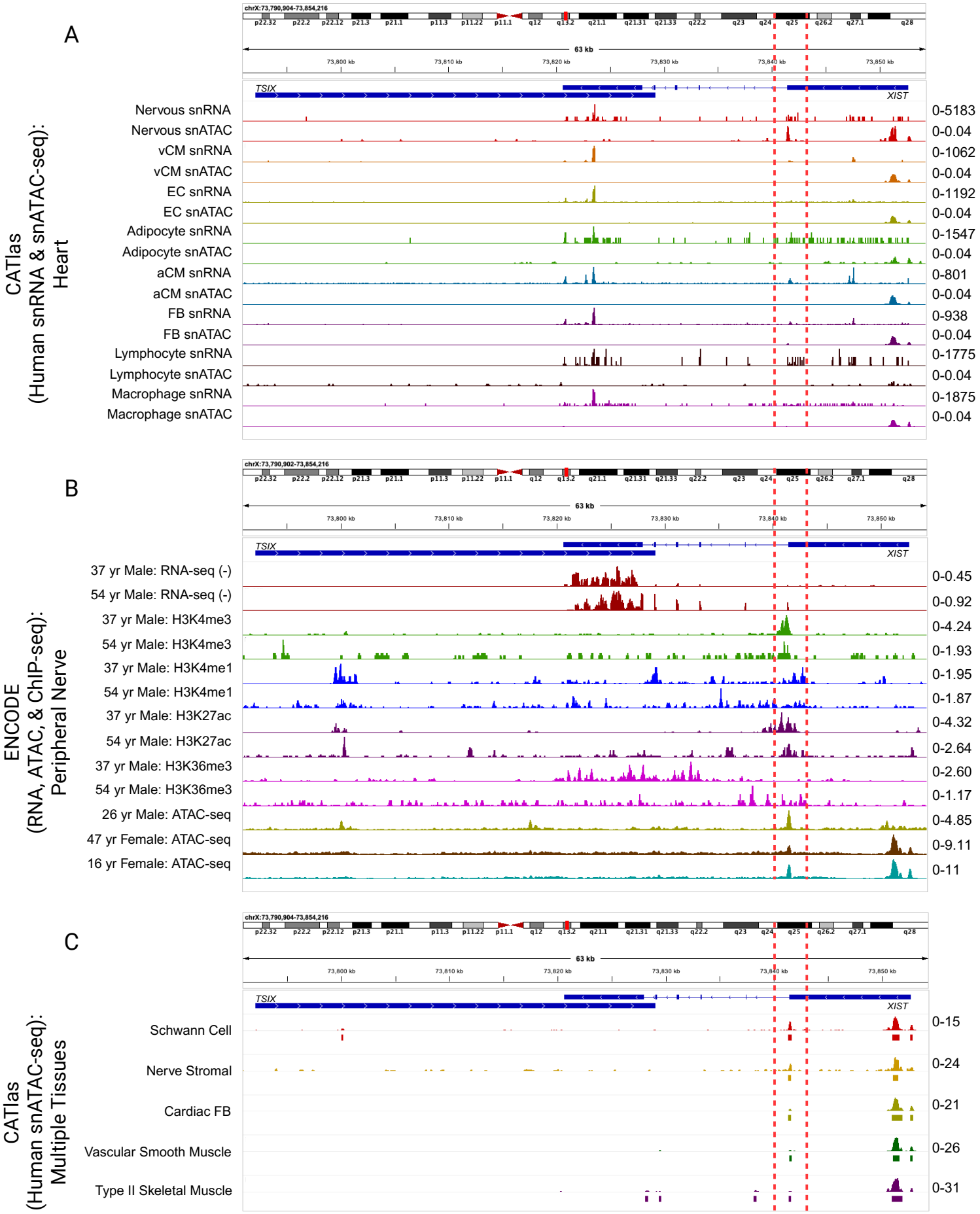
A
CATlas
(Human snRNA & snATAC-seq):
Heart
chrX:73,790,904-73,854,216
63 kb
73,800 kb
73,810 kb
73,820 kb
73,830 kb
73,840 kb
73,850 kb
TSIX
XIST
Nervous snRNA
Nervous snATAC
vCM snRNA
vCM snATAC
EC snRNA
EC snATAC
Adipocyte snRNA
Adipocyte snATAC
aCM snRNA
aCM snATAC
FB snRNA
FB snATAC
Lymphocyte snRNA
Lymphocyte snATAC
Macrophage snRNA
Macrophage snATAC
0-5183
0-0.04
0-1062
0-0.04
0-1192
0-0.04
0-1547
0-0.04
0-801
0-0.04
0-938
0-0.04
0-1775
0-0.04
0-1875
0-0.04
B
ENCODE
(RNA, ATAC, & ChIP-seq):
Peripheral Nerve
chrX:73,790,902-73,854,216
37 yr Male: RNA-seq (-)
54 yr Male: RNA-seq (-)
37 yr Male: H3K4me3
54 yr Male: H3K4me3
37 yr Male: H3K4me1
54 yr Male: H3K4me1
37 yr Male: H3K27ac
54 yr Male: H3K27ac
37 yr Male: H3K36me3
54 yr Male: H3K36me3
26 yr Male: ATAC-seq
47 yr Female: ATAC-seq
16 yr Female: ATAC-seq
0-0.45
0-0.92
0-4.24
0-1.93
0-1.95
0-1.87
0-4.32
0-2.64
0-2.60
0-1.17
0-4.85
0-9.11
0-11
C
CATlas
(Human snATAC-seq):
Multiple Tissues
chrX:73,790,904-73,854,216
Schwann Cell
Nerve Stromal
Cardiac FB
Vascular Smooth Muscle
Type II Skeletal Muscle
0-15
0-24
0-21
0-26
0-31

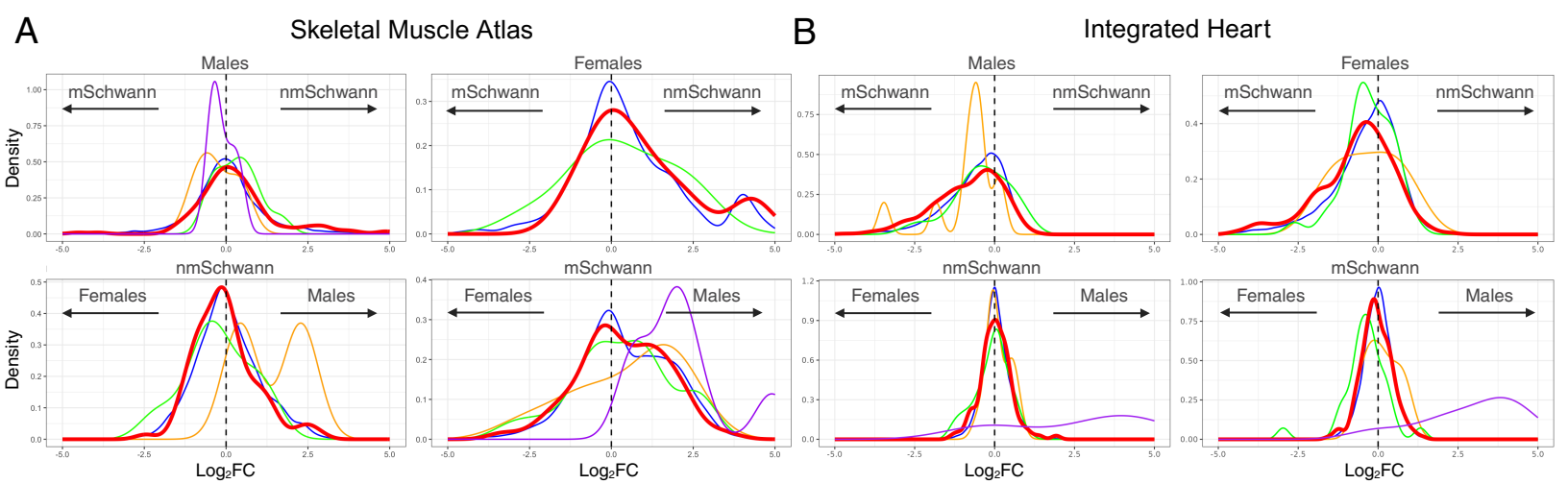

Expected (E) and observed (O) trends (LS: left shift, RS: right shift, NS: no shift, NA: no genes)

Gene Group	Top Left (A/B)	Top Right (A/B)	Bottom Left (A/B)	Bottom Right (A/B)
X Non-Escapee X Escapee PAR Y Non-PAR Autosomal	E: LS O: NS/LS E: NS O: RS/LS E: NS O: LS/LS E: NS O:LS/NA E: NS O:NS/LS	E: LS O: NS/LS E: NS O: NS/LS E: NS O: NA/NS E: NA O:NA/NA E: NS O:NS/NS	E: LS O: NS/NS E: NS O: LS/NS E: RS O: RS/NS E: RS O:NA/RS E: NS O:NS/NS	E: LS O: NS/NS E: NS O: RS/LS E: RS O: RS/NS E: RS O:RS/RS E: NS O:NS/NS

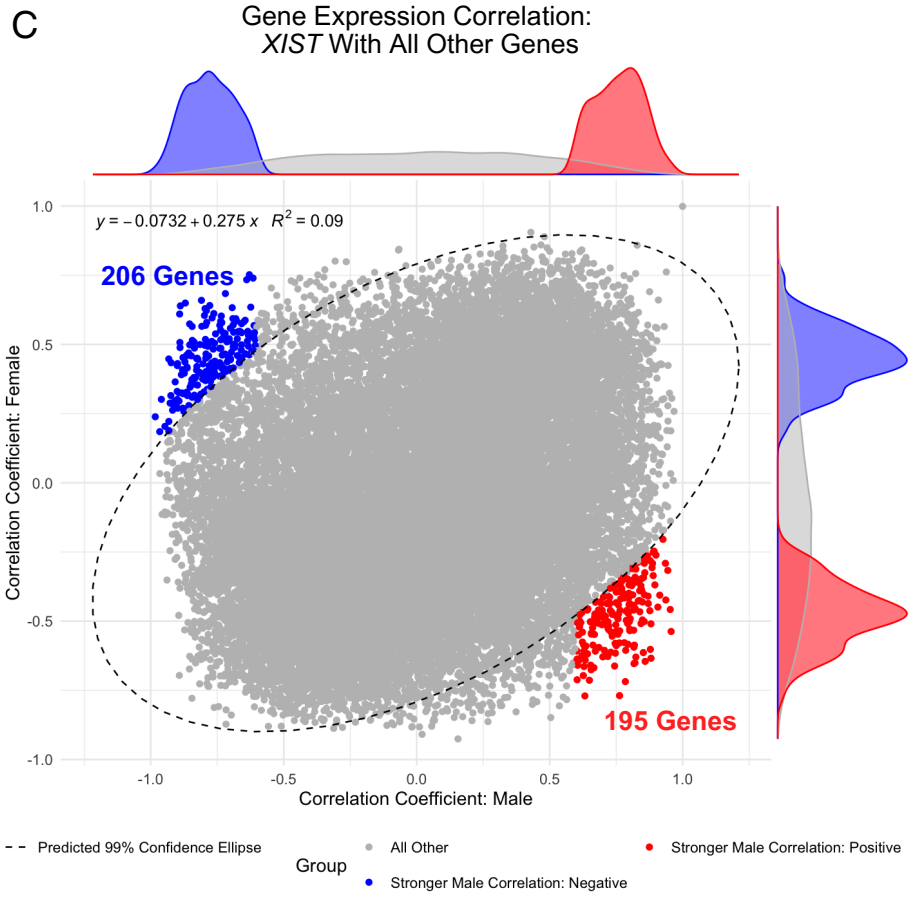

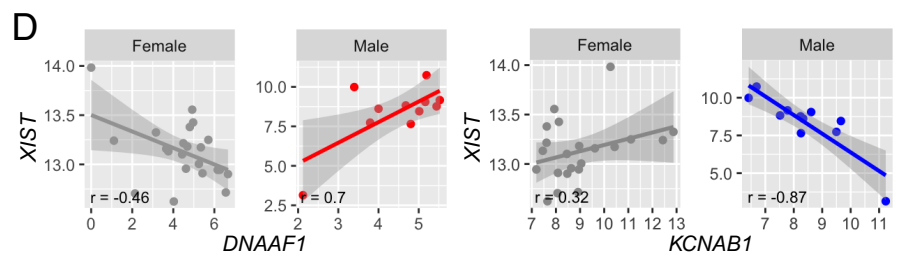

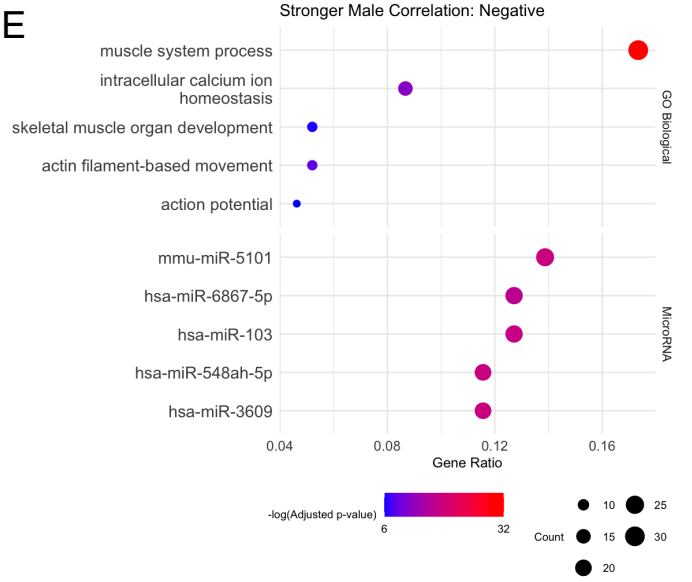

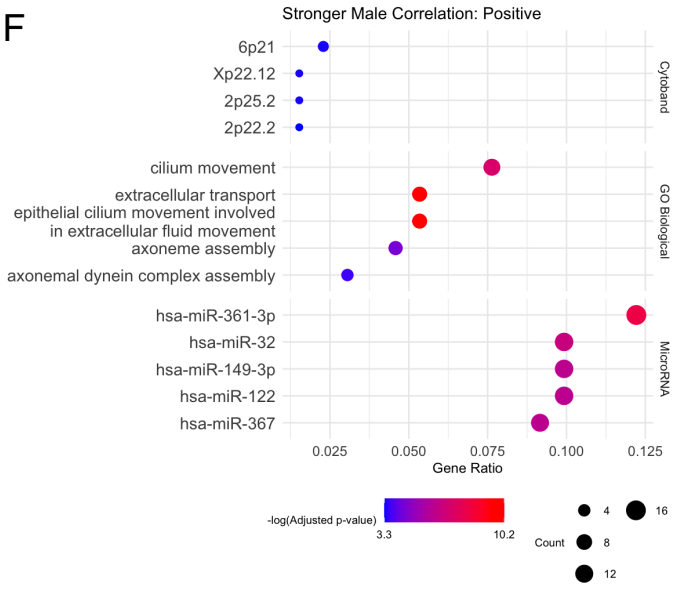

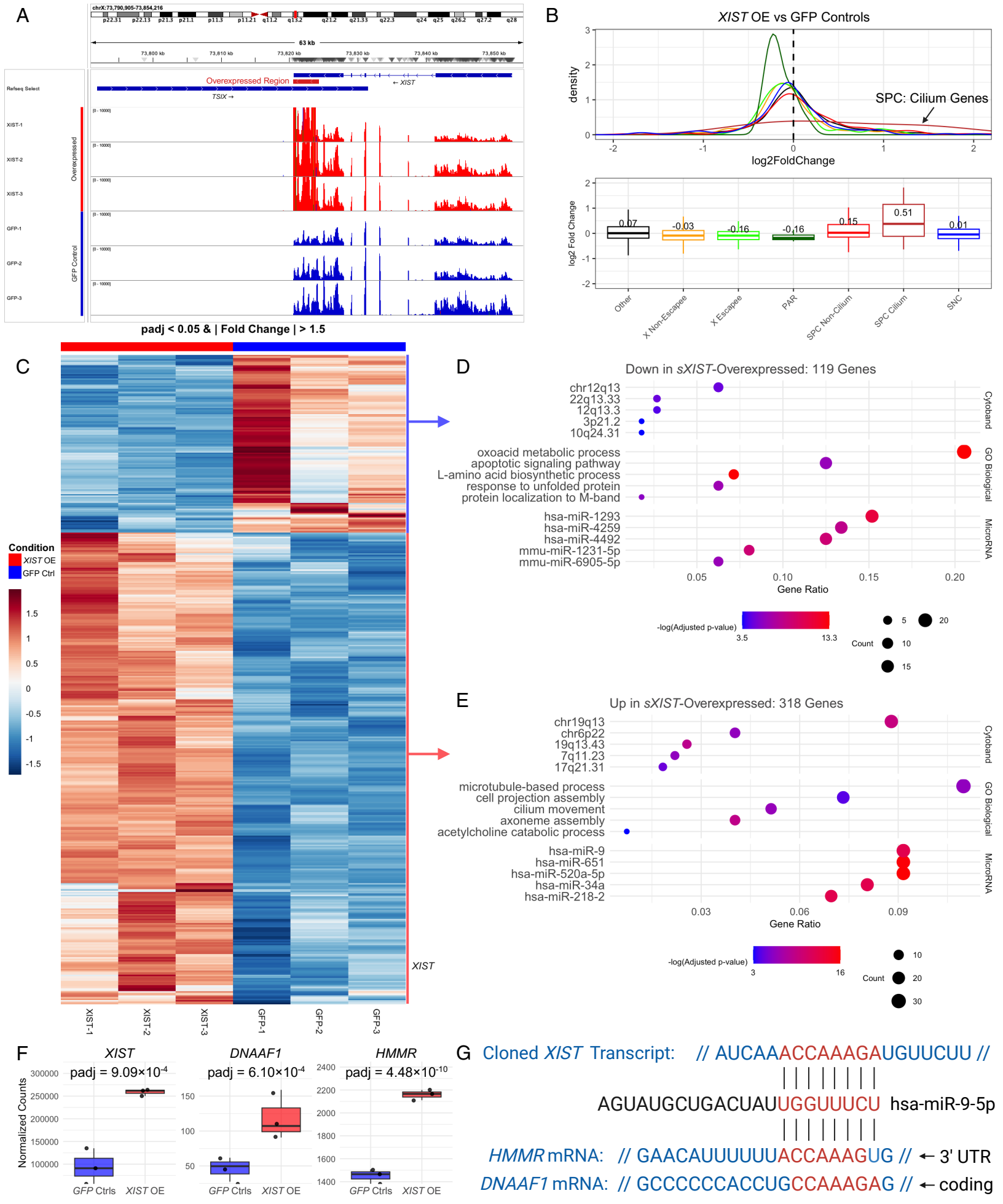
A
chrX:73,790,905-73,854,216
63 kb
Overexpressed Region
← XIST
TSIX →
Refseq Select
XIST-1
XIST-2
XIST-3
GFP-1
GFP-2
GFP-3
Overexpressed
GFP Control
padj < 0.05 & | Fold Change | > 1.5
B
XIST OE vs GFP Controls
density
log2FoldChange
SPC: Cilium Genes
log2 Fold Change
0.07
-0.03
-0.16
-0.16
0.15
0.51
0.01
Other
X Non-Escapee
X Escapee
PAR
SPC Non-Cilium
SPC Cilium
SNC
C
Condition
XIST OE
GFP Ctrl
XIST
XIST-1
XIST-2
XIST-3
GFP-1
GFP-2
GFP-3
D
Down in sXIST-Overexpressed: 119 Genes
chr12q13
22q13.33
12q13.3
3p21.2
10q24.31
oxoacid metabolic process
apoptotic signaling pathway
L-amino acid biosynthetic process
response to unfolded protein
protein localization to M-band
hsa-miR-1293
hsa-miR-4259
hsa-miR-4492
mmu-miR-1231-5p
mmu-miR-6905-5p
Cytoband
GO Biological
MicroRNA
Gene Ratio
-log(Adjusted p-value)
Count
E
Up in sXIST-Overexpressed: 318 Genes
chr19q13
chr6p22
19q13.43
7q11.23
17q21.31
microtubule-based process
cell projection assembly
cilium movement
axoneme assembly
acetylcholine catabolic process
hsa-miR-9
hsa-miR-651
hsa-miR-520a-5p
hsa-miR-34a
hsa-miR-218-2
Cytoband
GO Biological
MicroRNA
Gene Ratio
-log(Adjusted p-value)
Count
F
XIST
padj = 9.09×10-4
DNAAF1
padj = 6.10×10-4
HMMR
padj = 4.48×10-10
Normalized Counts
GFP Ctrls
XIST OE
G
Cloned XIST Transcript: // AUCAAACCAAAGAUGUUCUU //
AGUAUGCUGACUAUUGGUUUCU hsa-miR-9-5p
HMMR mRNA: // GAACAUUUUUUACCAAAGUG // ← 3' UTR
DNAAF1 mRNA: // GCCCCCCACCUGCCAAAGAG // ← coding

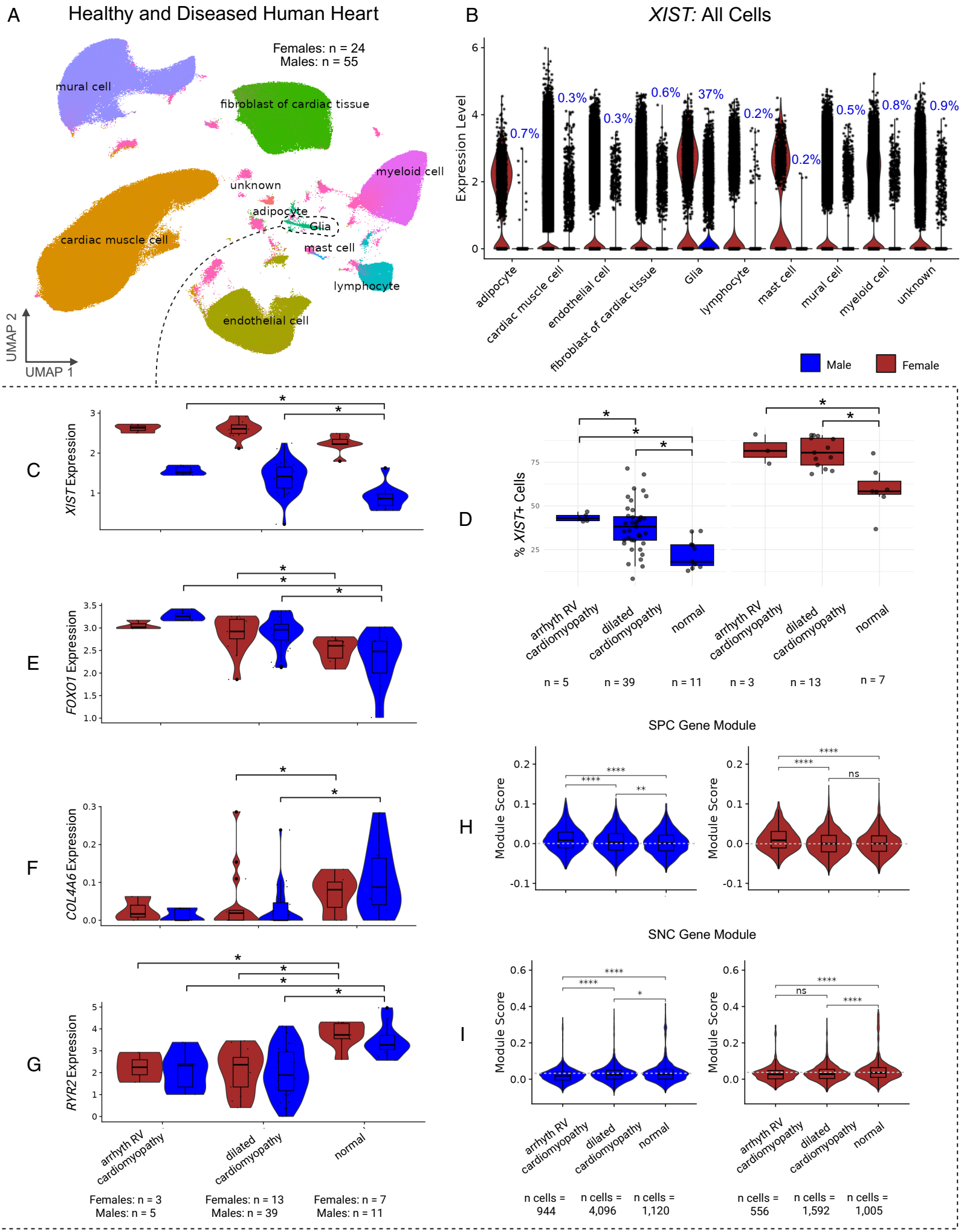

Transcription and potential functions of a novel *XIST* isoform in male peripheral glia

Kevin O'Leary, Meng-Yen Li, Kevyn Jackson, et al.

Genome Res. published online December 12, 2025
Access the most recent version at doi:10.1101/gr.280832.125